IEEE Access
Multidisciplinary | Rapid Review | Open Access Journal

Received May 18, 2022, accepted June 6, 2022, date of publication June 13, 2022, date of current version June 16, 2022.

Digital Object Identifier 10.1109/ACCESS.2022.3182552

Deep Learning-Assisted Power Minimization in Underlay MISO-SWIPT Systems Based On Rate-Splitting Multiple Access

MARIO R. CAMANA, (Graduate Student Member, IEEE), CARLA E. GARCIA, (Graduate Student Member, IEEE), AND INSOO KOO
Department of Electrical, Electronic and Computer Engineering, University of Ulsan, Ulsan 44610, South Korea

Corresponding author: Insoo Koo (iskoo@ulsan.ac.kr)

This work was supported in part by the National Research Foundation of Korea through the Korean Government Ministry of Science and Information and Communication Technologies (ICT) (MSIT) under Grant NRF-2021R1A2B5B01001721.

ABSTRACT In this article, we consider a multi-user multiple-input single-output underlay cognitive radio system with simultaneous wireless information and power transfer (SWIPT) based on the rate-splitting multiple access (RSMA) framework. The system model is composed of a set of secondary users that only decode information, and another set of secondary users that simultaneously decode information and harvest energy based on a power-splitting (PS) ratio. Precoders are designed to minimize the transmission power of the secondary transmitter subject to a minimum rate requirement, an energy harvesting requirement, and maximum allowable interference with the primary network. The optimization problem is non-convex and challenging. Thus, we divide it into two subproblems where the outer problem is solved by a deep neural network (DNN)-based scheme with an autoencoder, and the inner problem is solved based on the semidefinite relaxation (SDR) technique. The inner problem takes the solution of the DNN-based scheme to provide the precoder vectors and PS ratios based on SDR, where a penalty function is proposed to guarantee feasible solutions to the problems. Our simulation results prove that the proposed framework based on RSMA outperforms the conventional methods and can achieve performance close to that of the optimal solutions, with a significant reduction in computational complexity.

INDEX TERMS Rate-splitting (RS), simultaneous wireless information and power transfer (SWIPT), deep learning, cognitive radio network, semidefinite relaxation (SDR).

I. INTRODUCTION

Currently, the rapid increase in traffic demand expected from 5G and the incoming 6G technologies has promoted the development of new techniques to maximize the efficient use of wireless resources. In this respect, the concept of rate-splitting (RS) led to the development of rate-splitting multiple access (RSMA) [1], [2], which is a novel multiple access scheme based on the idea of splitting user messages into common and private parts. In RSMA, the common parts of messages are grouped into a super common message, which is encoded into a common stream based on a shared codebook, i.e., the common stream needs to be decoded by all users. The private parts of messages are independently encoded into separate streams by using private codebooks. Then, based on the channel state information at the transmitter (CSIT), the common and private streams are linearly precoded and superposed to be transmitted over the wireless channel. On the user side, RMSA uses the successive interference cancellation (SIC) procedure to first decode the common stream by considering the interference from the private streams as noise. Then, the super common message is re-encoded, precoded, and subtracted from the received signal to finally decode each intended private stream by considering the interference from other private streams as noise. The original message is reconstructed by joining the intended private message to its respective part in the super common message. The message-split ratio permits adjusting the amount of interference to be decoded by the user, which allows RSMA to partially decode the interference and partially treat it as noise. This key characteristic is used in the literature to promote RSMA as a general multiple

The associate editor coordinating the review of this manuscript and approving it for publication was Arun Prakash.

access method, with space division multiple access (SDMA) and non-orthogonal multiple access (NOMA) as special cases [2]–[4]. In SDMA and conventional multi-user linear precoding, the interference from other messages is fully treated as noise, whereas in NOMA, the interference from other messages is decoded by using several layers of SIC.

To improve spectral efficiency, cognitive radio (CR) is presented in the literature as a promising technique [5], [6]. In particular, we study the underlying cognitive radio system, which is composed of primary users (PUs) who share their spectrum band with a secondary network, provided that interference with the PUs is generated by secondary transmitters at less than a certain predetermined level. To overcome the power consumption problems of wireless devices, such as low-power IoT, one efficient technique is simultaneous wireless information and power transfer (SWIPT) [7], [8]. SWIPT combines radio frequency (RF) wireless energy transfer (WET) and wireless information transfer (WIT) by transmitting information and energy simultaneously. However, a trade-off between data rate and energy needs to be considered to achieve an efficient SWIPT scheme. Power-splitting (PS) is one of the most efficient structures to be used at the receiver, where the incoming signal is split into two parts, one to be used for information decoding (ID) and the other for energy harvesting (EH).

A. RELATED WORKS

An overview of SWIPT and its applications can be found in [7] and [8]. One of the first works considering SWIPT with a multiple-input single-output (MISO) system was proposed in [9] and was composed of users equipped with a PS structure. They addressed the minimization of total transmit power by optimizing the beamforming vectors and PS ratios. In [10], the authors considered a MIMO system in which several users implemented the PS structure. They try to minimize transmit power by jointly optimizing the beamforming vectors and PS ratios. In [11], energy-efficiency optimization was investigated in a MIMO system by considering a time-switching structure for SWIPT users but under constraints on maximum available power and minimum harvested energy. In a multi-user MISO system, the NOMA method was studied in [12] to maximize energy efficiency while optimizing beamforming vectors, subject to a minimum rate requirement. In [13], the NOMA method was used in a MISO SWIPT system composed of two users with cooperative transmission. The authors optimized the transmit beamformers and the PS ratio to maximize the data rate of the closer user, subject to a minimum rate for the farther user. In [14], the authors considered the maximization of the energy efficiency in a MIMO SWIPT relay network by assuming an imperfect knowledge of the channel vectors. The model of the channel errors was the norm bounded model, which is commonly used in the literature [15]. Moreover, the S-procedure [16] was applied in [14], [15] to deal with the infinite number of constraints caused by the imperfect CSI. The abovementioned works investigated SWIPT in a MISO system by applying SDMA or the NOMA technique without considering an underlying cognitive radio system.

In cognitive radio systems, the authors in [17] used the SDMA scheme in a CR MISO SWIPT system to minimize total transmit power from the secondary base station. The beamforming vectors and PS ratios are optimized by using the SDR technique, subject to rate, energy, and interference thresholds. In [18], a multi-user CR MISO SWIPT system with SDMA was proposed to investigate the max-min fair-harvested energy problem, subject to rate, energy, and interference constraints. In [5], underlay MISO–NOMA SWIPT was considered where secondary users are equipped with the PS structure. The authors studied the power minimization problem to optimize transmit beamforming vectors and PS ratios under rate, energy, and interference constraints, where the SDR technique with an iterative penalty method was used to solve the problem. A MISO–NOMA cognitive radio system with SWIPT was investigated in [6] under imperfect CSIT, where the secondary receiver architecture relies on a PS design. The authors considered a minimum transmission power problem and a maximum energy harvesting problem to optimize the precoding vectors, the energy vector, and the PS ratio. The solution was based on SDR and a one-dimensional search algorithm. Moreover, NOMA in a CR system has been applied in physical layer security to minimize the transmission power [19], [20] and maximize the secrecy sum rate [21].

In the aforementioned works, only the conventional SDMA and NOMA methods were considered. The RS method was introduced in [1] as a novel physical-layer strategy that is capable of providing improvement in spectral and energy efficiency, compared with traditional methods. In [22], the RS strategy was applied in a multi-user MISO system under imperfect CSIT. The authors studied the max-min fairness problem, where the weighted minimum mean square error (WMMSE) approach was used to obtain solutions. The simulation results proved that the RS-based approach achieved a higher rate, compared with traditional designs. The RS strategy was applied in a massive MIMO system in [23] by considering imperfect CSIT to maximize the minimum rate achieved with the common message. In [24], the RS method was implemented in a MISO unicast and multicast system. RS exploited the existing SIC structure by combining the common part of a unicast message with a multicast message to maximize both the weighted sum rate and energy efficiency. The RSMA framework was introduced in [2] for a downlink, multi-user MISO system. The authors investigated the weighted sum-rate maximization problem subject to a minimum rate requirement and a power constraint, in which the solution was based on the WMMSE approach. The authors described the limitations in the conventional SDMA and NOMA methods, and presented RSMA as a more powerful and general method, with SDMA and NOMA as special cases. Simulation results proved the authors' claims and the superior performance of RSMA over conventional frameworks. In [3],

a two-user MISO system was considered for sum-rate analysis in order to show analytically that the conventional methods of orthogonal multiple access (OMA), NOMA, and SDMA are special cases of the RS framework. In [25], energy efficiency maximization in a multi-user MISO system with RS was studied, and the trade-off between spectral and energy efficiency was investigated in [26]. Both studies showed that RSMA is more spectral- and energy-efficient, compared with NOMA and SDMA. In [4], the authors provided a discussion of RS as a potential candidate for future 6G multi-antenna systems. The authors showed how RSMA can address the requirements of data rate, latency, reliability, mobility, and energy efficiency. They highlighted the robustness of RSMA in dealing with different kinds of imperfect CSIT, and showed the flexibility it has in dealing with several types of traffic, such as unicast, multicast, and broadcast. Moreover, it was claimed that RSMA permits reducing the complexity at the receiver, since only one layer of SIC is required (compared with the several SIC layers needed in NOMA) while achieving higher performance.

The RS strategy was considered in [27] for a multi-user MISO SWIPT system composed of users that only decode information and users that only harvest energy. The precoder vectors and the common rate variables were optimized to maximize the weighted sum rate under a minimum energy-harvesting requirement and maximum transmission power, where WMMSE and a successive convex approximation (SCA)-based algorithm were proposed to solve the problem. In [28], a MISO interference channel with SWIPT and RS was considered under imperfect CSIT. The authors considered transmit power minimization to obtain the beamforming vectors and PS ratios, subject to rate and energy constraints. The solution was an iterative gradient algorithm that solves a semi-definite programming (SDP) problem in each step. In our previous work [29], a multi-user SWIPT system was investigated to minimize the transmission power, subject to rate and energy constraints. The precoder vectors, common rate variables, and PS ratios were optimized by a particle swarm optimization (PSO) algorithm along with the SDR approach. Note that the above articles did not consider a system with cognitive radio capabilities. In [30], we considered a multi-user MISO SWIPT system with RSMA and CR capabilities by assuming two types of users. The minimum transmit power problem was investigated subject to rate, energy, and interference constraints in which a PSO–SDR-based algorithm was proposed to solve the optimization problem. The simulation results showed a significant improvement achieved by the RSMA method over the conventional SDMA scheme. However, the PSO–SDR algorithm is an iterative method that increases computational complexity for RSMA, compared with the conventional methods. Then, it is crucial to investigate novel schemes with lower computational complexity to solve the optimization problems in SWIPT RSMA systems.

In the literature, deep learning is a promising method to approximate the optimization algorithms or to accelerate some of their steps, with the objective being to reduce computational complexity [31], [32]. The capabilities of different machine learning types and their limitations were discussed in [33] where a cognitive learning (CL) framework with adaptation capabilities for dynamic environments, was introduced in order to improve the quality of the decisions. The CL framework was used in the modulation recognition problem by selecting the most appropriate modulation recognition algorithm and its optimal parameters. In [34], the authors proposed a deep neural network (DNN)-based approach to approximate the WMMSE algorithm that solves the weighted sum-rate maximization problem in a network composed of several single-antenna transceiver pairs. The input for the DNN was the magnitude of the channel coefficients, and the output was the power allocation variables. The simulation results showed that good accuracy was achieved, with a significant reduction in computational time. In [35], an underlying CR network system was considered where the secondary network was composed of a single-antenna cognitive base station (CBS) and one secondary user. The authors optimized the transmit power of the CBS to maximize the transmission rate and energy efficiency. A deep neural network was used to approximate the optimal solution for both optimization problems where simulation results showed that the DNN-based scheme achieved a close performance to conventional methods with a significant decrease in the computational time. In [36], the authors considered a multi-user MISO system, and developed a deep learning–based approach to solving the power minimization problem, the signal-to-interference-plus-noise ratio (SINR) balancing problem, and the sum-rate maximization problem. The approach has two parts: the deep learning module and the beamforming recovery module. The deep learning module is composed of convolutional layers and fully connected layers, which provide key features to the beamforming recovery module. The key features are converted to a beamforming matrix based on expert knowledge of beamforming optimization. However, the beamforming recovery module and the design of the key features are problem-dependent, and cannot be directly used in other complex systems.

B. MAIN CONTRIBUTIONS

Motivated by the significant improvement from RSMA over traditional methods in spectral and energy efficiency in the literature, we consider an underlying MISO-SWIPT system composed of a set of secondary users that only decode information, with another set of secondary users equipped with the PS structure to simultaneously decode information and harvest energy. We propose a low-complexity approach to optimize the precoder vectors, the common rate variables, and the PS ratios while minimizing the transmission power at the secondary transmitter (STx).

The generalization performance of deep learning schemes measures the ability of the model to perform well in testing data which is significantly different from the training data. This issue is of great importance because in real-world

implementations the deep learning scheme may cause infeasible or suboptimal solutions leading to performance degradation. Therefore, in this paper, we propose a DNN-SDR approach assisted with an autoencoder where channel vectors, rate thresholds, and energy thresholds are considered as input parameters. Then, we analyze the generalization performance of the proposed model for different scenarios not included in the training data without the need to retrain the DNN model. The main contributions of this paper are summarized as follows:

- We propose a novel, deep learning–based approach for solving the power minimization problem in a CR MISO SWIPT system with RSMA, subject to constraints on the minimum rate requirement, the minimum EH requirement, and the maximum allowable interference with the primary network. The proposed solution is composed of an autoencoder for dimensionality reduction, a DNN to find the common rate variables, and an SDR module to obtain the precoder vectors and PS ratios.
- Given the common rate variables by the DNN, the SDR technique with a penalty method is used to solve the non-convex problem in the SDR module, in which all the constraints are being satisfied.
- We consider the scenario with imperfect knowledge of the channel vectors by assuming a bounded CSI error model. A robust precoding design is proposed to deal with the imperfect CSIT, where the proposed solution is based on the S-procedure and the SDR technique.
- For comparison purposes, we developed a NOMA-based scheme to solve power minimization in the considered system model, where the close-to-optimal solution is based on the SDR technique.
- Numerical simulations are presented to evaluate the performance of the RSMA method over the conventional SDMA and NOMA schemes. We prove the generalization capability of the proposed approach in several scenarios, such as different signal attenuations, different numbers of transmitting antennas, and imperfect CSIT, which are not considered during the training process. Moreover, we show that the proposed approach based on deep learning permits a major reduction in computational complexity, compared with the close-to-optimal scheme, while achieving similar performance.

The rest of the paper is organized as follows. Section II illustrates the system model. Section III presents the problem formulation, the proposed DNN-based solution, the SDR approach to the problem, and the comparative NOMA scheme. Simulation results are illustrated in Section IV, followed by conclusions in Section V.

Notations: The matrices and vectors are represented by bold uppercase and lowercase letters, respectively. The transpose and conjugate transpose, respectively, are denoted as $(\cdot)^T$ and $(\cdot)^H$. The trace of a matrix is represented by $\mathrm{Tr}(\cdot)$, the expectation is denoted as $\mathbb{E}\{\cdot\}$, and $|\cdot|$ and $\|\cdot\|$ refer to the absolute value and the Euclidean norm, respectively.

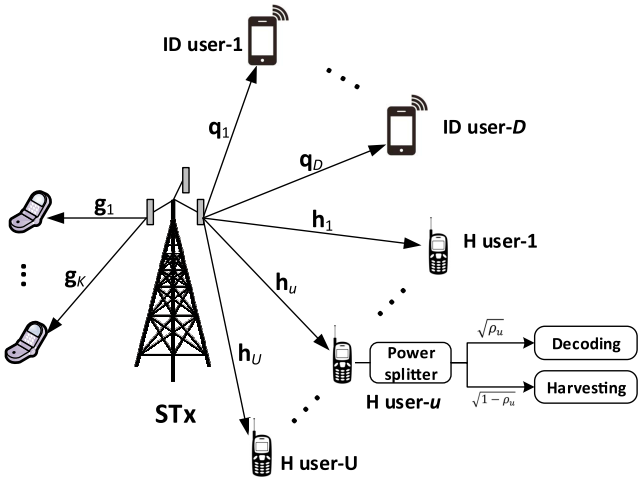

FIGURE 1. Architecture of the underlay MISO-SWIPT system.

$\mathcal{CN}(\mu, \sigma^2)$ represents the circularly symmetric complex Gaussian (CSCG) distribution with mean μ and variance σ^2.

II. SYSTEM MODEL

We investigate a multi-user MISO cognitive radio system with SWIPT by using the RSMA method. The system model is composed of U hybrid users equipped with a PS structure to simultaneously decode information and harvest energy, plus D users with the ability to only decode information, denoted as ID users, and K PUs, as illustrated in Fig. 1. We consider an STx with $N \geq 2$ antennas, while the U hybrid users, D ID users, and K PUs each have a single antenna. We denote as $\mathbf{h}_u \in \mathbb{C}^{N\times 1}$ the channel vector between the STx and the u-th hybrid user; $\mathbf{q}_d \in \mathbb{C}^{N\times 1}$ denotes the channel vector between the STx and the d-th ID receiver, and $\mathbf{g}_k \in \mathbb{C}^{N\times 1}$ is the channel vector from the STx to the k-th PU.

We propose an RS strategy for the multiple access method, known as RSMA in the literature, to satisfy the rate and energy requirements in the system. The one-layer RS requires one SIC in the receiver, which reduces the number of SIC layers at the receiver, compared to NOMA. The message for the u-th hybrid user is denoted as m_u^H, which is split into a common message, $m_u^{H,c}$, and a private message, $m_u^{H,p}$. Similarly, the message for the d-th ID user is denoted as m_d^{ID}, in which the common and private parts are $m_d^{ID,c}$ and $m_d^{ID,p}$, respectively.

In RSMA, the common parts of the original messages intended for the hybrid and ID users, i.e. $\{m_1^{H,c}, \ldots, m_U^{H,c}, m_1^{ID,c}, \ldots, m_D^{ID,c}\}$, are grouped and jointly encoded into common stream s_c with $\mathbb{E}\{|s_c|^2\} = 1$, as illustrated in Fig. 2. The private parts of the messages intended for the hybrid users, $\{m_1^{H,p}, \ldots, m_U^{H,p}\}$, are independently encoded into private streams $\{s_1^H, \ldots, s_U^H\}$ with $\mathbb{E}\{|s_u^H|^2\} = 1$. Similarly, the private parts of the messages intended for the ID users, $\{m_1^{ID,p}, \ldots, m_D^{ID,p}\}$, are independently encoded into private streams $\{s_1^{ID}, \ldots, s_D^{ID}\}$ with $\mathbb{E}\{|s_d^{ID}|^2\} = 1$. The precoder

vectors for streams s_c, s_u^H, and s_d^{ID} are defined as $\mathbf{w}_c \in \mathbb{C}^{N\times 1}$, $\mathbf{w}_u \in \mathbb{C}^{N\times 1}$, and $\mathbf{v}_d \in \mathbb{C}^{N\times 1}$, respectively. The transmit signal is given by

$$\mathbf{x} = \mathbf{w}_c s_c + \sum_{u=1}^{U} \mathbf{w}_u s_u^H + \sum_{d=1}^{D} \mathbf{v}_d s_d^{ID}. \tag{1}$$

At the hybrid and ID receivers, the first step is decoding common stream s_c by treating interference from the private messages as noise. The hybrid users with the PS structure divide the received signal into two power streams based on PS ratio $\rho_u \in (0, 1)$, where one power stream is sent to an ID module, and the other power stream is sent to the EH module. Thus, at the u-th hybrid user, the achievable rate of common stream s_c is given by

$$R_{u,c}^H = \log_2\left(1+\frac{\rho_u\left|\mathbf{h}_u^H\mathbf{w}_c\right|^2}{\rho_u\left(\sum_{i=1}^{U}\left|\mathbf{h}_u^H\mathbf{w}_i\right|^2+\sum_{d=1}^{D}\left|\mathbf{h}_u^H\mathbf{v}_d\right|^2+\sigma_{H,u}^2\right)+\gamma_u^2}\right), \quad \forall u, \tag{2}$$

while $n_u^H \sim \mathcal{CN}(0, \sigma_{H,u}^2)$ is additive white Gaussian noise (AWGN) at the u-th hybrid user, and $\vartheta_u \sim \mathcal{CN}(0, \gamma_u^2)$ is the circuit noise at the ID component of the u-th hybrid user. The SIC layer is applied after decoding common stream s_c, where private stream s_u^H is decoded by treating the interference caused by other private messages as noise. Then, the achievable rate of private stream s_u^H at the u-th hybrid user is (3), as shown at the bottom of the next page.

At the d-th ID user, the achievable rate of common stream s_c is given by

$$\mathrm{R}_{d,c}^{ID} = \log_2\left(1+\frac{\left|\mathbf{q}_d^H\mathbf{w}_c\right|^2}{\sum_{u=1}^{U}\left|\mathbf{q}_d^H\mathbf{w}_u\right|^2+\sum_{j=1}^{D}\left|\mathbf{q}_d^H\mathbf{v}_j\right|^2+\sigma_{ID,d}^2}\right), \quad \forall d, \tag{4}$$

where $n_d^{ID} \sim \mathcal{CN}(0, \sigma_{ID,d}^2)$ is AWGN at the d-th ID user. Once common stream s_c is successfully decoded, we can apply the SIC procedure, and the achievable rate of private stream s_d^{ID} at the d-th ID user is given by

$$\mathrm{R}_{d}^{ID} = \log_2\left(1+\frac{\left|\mathbf{q}_d^H\mathbf{v}_d\right|^2}{\sum_{u=1}^{U}\left|\mathbf{q}_d^H\mathbf{w}_u\right|^2+\sum_{j=1,j\neq d}^{D}\left|\mathbf{q}_d^H\mathbf{v}_j\right|^2+\sigma_{ID,d}^2}\right), \quad \forall d. \tag{5}$$

We define a common rate, R_c, at which common stream s_c is transmitted, where R_c must not exceed the achievable rate of s_c at the weakest hybrid and ID users, i.e. $R_c = \min\left\{R_{1,c}^H, \ldots, R_{U,c}^H, R_{1,c}^{ID}, \ldots, R_{D,c}^{ID},\right\}$. The total rate of the u-th hybrid user is given by $\mathrm{R}_u^H + \mathrm{r}_{u,c}^H$, where $\mathrm{r}_{u,c}^H$ is the rate of the common part of the original message of the u-th hybrid user, i.e. $m_u^{H,c}$. Similarly, the total rate of the d-th ID user is given by $\mathrm{R}_d^{ID} + \mathrm{r}_{d,c}^{ID}$, where $\mathrm{r}_{d,c}^{ID}$ is the rate of the common part of the original message of the d-th ID user, i.e. $m_d^{ID,c}$. Then, R_c can be expressed as

$$R_c = \sum_{u=1}^{U} r_{u,c}^H + \sum_{d=1}^{D} r_{d,c}^{ID}. \tag{6}$$

At the u-th hybrid user, the energy harvested at the EH component is computed as

$$E_u^H = \eta_u(1-\rho_u)\left(\left|\mathbf{h}_u^H\mathbf{w}_c\right|^2+\sum_{i=1}^{U}\left|\mathbf{h}_u^H\mathbf{w}_i\right|^2+\sum_{d=1}^{D}\left|\mathbf{h}_u^H\mathbf{v}_d\right|^2+\sigma_{H,u}^2\right), \quad \forall u, \tag{7}$$

where the energy-harvesting efficiency of the u-th hybrid user is denoted by $\eta_u \in (0, 1]$.

The interference power at the k-th PU user from the STx is given by

$$\mathrm{P}_k^{\mathrm{int}} = \left|\mathbf{g}_k^H\mathbf{w}_c\right|^2+\sum_{u=1}^{U}\left|\mathbf{g}_k^H\mathbf{w}_u\right|^2+\sum_{d=1}^{D}\left|\mathbf{g}_k^H\mathbf{v}_d\right|^2, \quad \forall k. \tag{8}$$

III. PROBLEM FORMULATION AND SOLUTION

A. PROBLEM FORMULATION

In this paper, we aim to minimize the total transmit power at the STx by optimizing the precoder vectors, the PS ratios, and the common rate variables. The optimization problem proposed in this paper is formulated as follows:

$$\min_{\mathbf{w}_c,\left\{\mathbf{w}_u,\mathbf{v}_d,r_{u,c}^H,r_{d,c}^{ID},\rho_u\right\}} \|\mathbf{w}_c\|^2+\sum_{u=1}^{U}\|\mathbf{w}_u\|^2+\sum_{d=1}^{D}\|\mathbf{v}_d\|^2 \tag{9a}$$

$$\text{s.t. C1: } r_{u,c}^H + R_u^H \geq R_{u,\min}^H, \quad \forall u \tag{9b}$$

$$\text{C2: } r_{d,c}^{ID} + R_d^{ID} \geq R_{d,\min}^{ID}, \quad \forall d \tag{9c}$$

$$\text{C3: } \sum_{i=1}^{U} r_{i,c}^H + \sum_{d=1}^{D} r_{d,c}^{ID} \leq R_{u,c}^H, \quad \forall u \tag{9d}$$

$$\text{C4: } \sum_{u=1}^{U} r_{u,c}^H + \sum_{j=1}^{D} r_{j,c}^{ID} \leq R_{d,c}^{ID}, \quad \forall d \tag{9e}$$

$$\text{C5: } \mathrm{E}_u^H \geq \psi_u, \quad \forall u \tag{9f}$$

$$\text{C6: } \|\mathbf{w}_c\|^2+\sum_{u=1}^{U}\|\mathbf{w}_u\|^2+\sum_{d=1}^{D}\|\mathbf{v}_d\|^2 \leq P_{\max} \tag{9g}$$

$$\text{C7: } \mathrm{P}_k^{\mathrm{int}} \leq \chi_k, \quad \forall k \tag{9h}$$

$$\text{C8: } 0 < \rho_u < 1, \ \forall u \tag{9i}$$

$$\text{C9: } r_{u,c}^H \geq 0, r_{d,c}^{ID} \geq 0, \quad \forall u, \ \forall d, \tag{9j}$$

where $P_{\max}$ represents the maximum transmit power of the STx, ψ_u denotes the minimum harvested energy required at the u-th hybrid user, χ_k represents the maximum tolerable

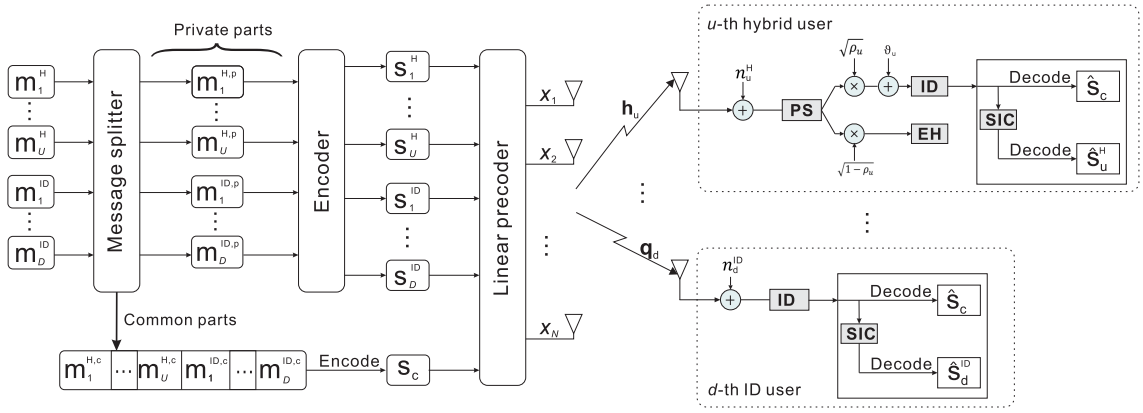

FIGURE 2. Rate-splitting framework for the proposed system model.

interference power of the k-th PU, and $R^{H}_{u,\min}$ and $R^{ID}_{d,\min}$ are the minimum rate requirements of the hybrid and ID users, respectively. In (9b)-(9h), C1 and C2 guarantee the minimum rate requirement for the messages of the hybrid and ID users; C3 and C4 guarantee that common stream s_c is effectively decoded by the hybrid and ID users; and C5 establishes the minimum harvested requirement at the hybrid users. C6 limits the maximum transmission power at the STx, and C7 restricts the power level for interference with the PUs.

Problem (9) is difficult to solve due to non-convex constraints C1 to C5. Thus, we divide main problem (9) into two subproblems, and propose a DNN–SDR solution to solve them.

First, a DNN-based approach is used to obtain the common rate variables, $\left\{r^{H}_{u,c}, r^{ID}_{d,c}\right\}$, based on the channel vectors, rate, and energy requirements, as detailed in Section III.B. Then, given the fixed rate variables, $r^{H}_{u,c}$ and $r^{ID}_{d,c}$, problem (9) can be simplified to

$$\min_{\mathbf{w}_c,\{\mathbf{w}_u,\mathbf{v}_d,\rho_u\}} \|\mathbf{w}_c\|^2 + \sum_{u=1}^{U} \|\mathbf{w}_u\|^2 + \sum_{d=1}^{D} \|\mathbf{v}_d\|^2 \tag{10a}$$

subject to:

$$\frac{\left|\mathbf{h}_u^H \mathbf{w}_u\right|^2}{\sum_{i=1,i\neq u}^{U} \left|\mathbf{h}_u^H \mathbf{w}_i\right|^2 + \sum_{d=1}^{D} \left|\mathbf{h}_u^H \mathbf{v}_d\right|^2 + \sigma^2_{H,u} + \frac{\gamma_u^2}{\rho_u}} \geq \alpha_u^H, \ \forall u \tag{10b}$$

$$\frac{\left|\mathbf{q}_d^H \mathbf{v}_d\right|^2}{\sum_{u=1}^{U} \left|\mathbf{q}_d^H \mathbf{w}_u\right|^2 + \sum_{j=1,j\neq d}^{D} \left|\mathbf{q}_d^H \mathbf{v}_j\right|^2 + \sigma^2_{ID,d}} \geq \alpha_d^{ID}, \ \forall d \tag{10c}$$

$$\frac{\left|\mathbf{h}_u^H \mathbf{w}_c\right|^2}{\sum_{i=1}^{U} \left|\mathbf{h}_u^H \mathbf{w}_i\right|^2 + \sum_{d=1}^{D} \left|\mathbf{h}_u^H \mathbf{v}_d\right|^2 + \sigma^2_{H,u} + \frac{\gamma_u^2}{\rho_u}} \geq \beta, \ \forall u \tag{10d}$$

along with (9f), (9g), (9h) and (9i),

$$\frac{\left|\mathbf{q}_d^H \mathbf{w}_c\right|^2}{\sum_{u=1}^{U} \left|\mathbf{q}_d^H \mathbf{w}_u\right|^2 + \sum_{j=1}^{D} \left|\mathbf{q}_d^H \mathbf{v}_j\right|^2 + \sigma^2_{ID,d}} \geq \beta, \ \forall d \tag{10e}$$

where $\beta = 2^{\sum_{i=1}^{U} r^{H}_{i,c} + \sum_{d=1}^{D} r^{ID}_{d,c}} - 1$, $\alpha_u^H = \max\left\{0, 2^{R^{H}_{u,\min} - r^{H}_{u,c}} - 1\right\}$, and $\alpha_d^{ID} = \max\left\{0, 2^{R^{ID}_{d,\min} - r^{ID}_{d,c}} - 1\right\}$. Problem (10) is still a non-convex problem. Then, we propose solving problem (10) based on the SDR technique in Subsection III.C, and we present the NOMA method as a comparative approach to solving main problem (9) in Subsection III.D.

The proposed scheme can be used to minimize the total power consumption at the STx by modifying the objective function (9a) to the following [24]:

$$P_T^{STx} = \Phi P_{STx} + P_{c,ant} N + P_{st}, \tag{11}$$

where P_T^{STx} is the total power consumption at the STx, $P_{STx} = \|\mathbf{w}_c\|^2 + \sum_{u=1}^{U} \|\mathbf{w}_u\|^2 + \sum_{d=1}^{D} \|\mathbf{v}_d\|^2$, $\Phi \geq 1$ represents the power inefficiency of the power amplifier, $P_{c,ant}$ represents the circuit power consumption due to each antenna in the STx, and P_{st} is the static circuit power consumption, which is independent of the transmitted power. Typical values for the aforementioned parameters are $\Phi = 2.85$, $P_{c,ant} = 27$ dBm, and $P_{ct} = 30$ dBm [24]. Since the values of Φ, $P_{c,ant}$, and

$$\mathrm{R}_u^H = \log_2\left(1 + \frac{\rho_u \left|\mathbf{h}_u^H \mathbf{w}_u\right|^2}{\rho_u\left(\sum_{i=1,i\neq u}^{U} \left|\mathbf{h}_u^H \mathbf{w}_i\right|^2 + \sum_{d=1}^{D} \left|\mathbf{h}_u^H \mathbf{v}_d\right|^2 + \sigma^2_{H,u}\right) + \gamma_u^2}\right), \quad \forall u. \tag{3}$$

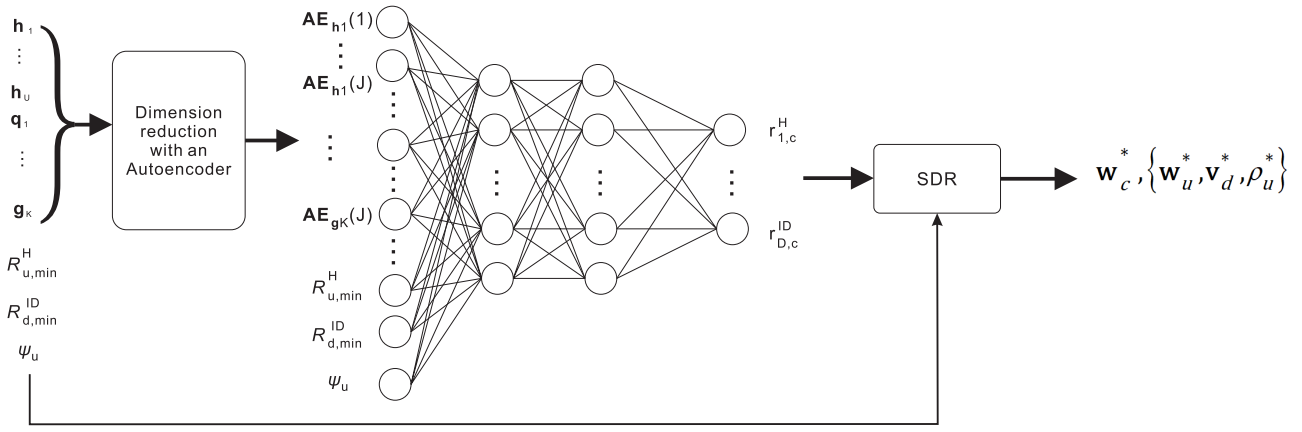

FIGURE 3. General structure of the proposed DNN–SDR based scheme.

P_{st} can be considered constant, the total power consumption is defined and directly proportional to P_{STx}.

B. DNN-BASED ALGORITHM TO OBTAIN THE COMMON RATES

In this paper, we propose a DNN-based scheme with an autoencoder to obtain the approximate optimal values of the common rate variables in problem (9). In particular, we find the values for common rate variable $\{r^H_{u,c}\}$ of the u-th hybrid user and for common rate variable $\left\{r^{ID}_{d,c}\right\}$ of the d-th ID user. Fig. 3 shows the structure of the proposed method. The proposed approach is composed of three main modules: an autoencoder, a DNN, and an SDR module to solve problem (10).

The elements of the channel vectors in a MISO system depend on the number of antennas, where each element is composed of a real part and an imaginary part. Then, as the number of users and antennas increases, so does the total input required at the DNN while increasing the complexity required at the DNN module. For instance, considering eight antennas at the STx and six total users, we have 96 inputs just due to the channel vectors, and if we increase the number of antennas to 28, we have 336 inputs due to the channel vectors. Therefore, we propose an autoencoder as the first module, which is in charge of reducing the dimension of the channel vectors and dealing with the imaginary part. In particular, each channel vector from the STx to the users (hybrid, ID, and PUs) is independently encoded into a lower-dimensional representation and is used as input for the DNN. The first step of the process is to separate each element of the channel vectors into real and imaginary parts, i.e. the number of inputs for the autoencoder is $2 \times N$.

The autoencoder is an unsupervised learning method and a type of neural network composed of one input layer, an odd number of hidden layers, and an output layer with the same dimensions as the input layer. The general objective is to reproduce the data from the input layer to the output layer by passing through the hidden layers, while the reconstruction

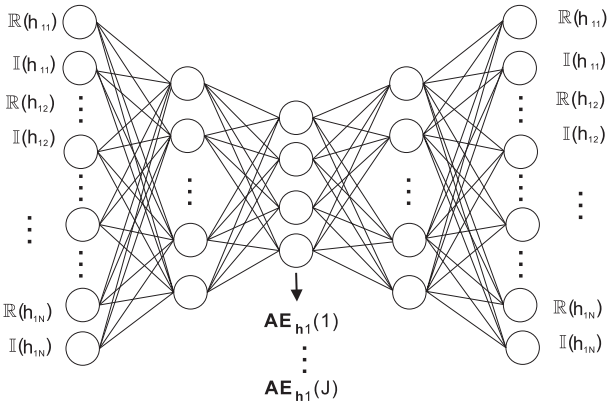

FIGURE 4. Example of the autoencoder module for channel vector $\mathbf{h}_1$.

error or loss function is used to optimize the weights of the network. For dimensionality reduction, the autoencoder is designed to have fewer units in the middle layer than in the input layer. In detail, we consider an M-layer autoencoder, where the m-th layer has the same number of units as the $(M - m + 1)$-th layer [37]. Then, we can divide the autoencoder into an encoder part, which includes the input layer to the $(M+1)/2$-th layer and that is in charge of mapping the input data into a lower-dimensional representation, and a decoder part, which includes the $(M + 1)/2$-th layer to the output layer. The $(M + 1)/2$-th layer is the most constricted layer, where the reduced representation of the input data is obtained. Fig. 4 illustrates an example of the proposed autoencoder-based scheme for dimensionality reduction, composed of three hidden layers, where the input is represented by the real and imaginary parts of the channel vector, and the encoded state is the output of the second hidden layer (composed of J units). We denote as $\mathbf{AE}_{\mathbf{h}_u} \in \mathbb{R}^{Jx1}$ the reduced representation of channel vector $\mathbf{h}_u$. Similarly, $\mathbf{AE}_{\mathbf{q}_d}$ and $\mathbf{AE}_{\mathbf{g}_k}$ are the reduced representations of channel vectors $\mathbf{q}_d$ and $\mathbf{g}_k$, respectively.

The second module is a DNN composed of an input layer, M_{DNN} hidden layers, and an output layer, as illustrated

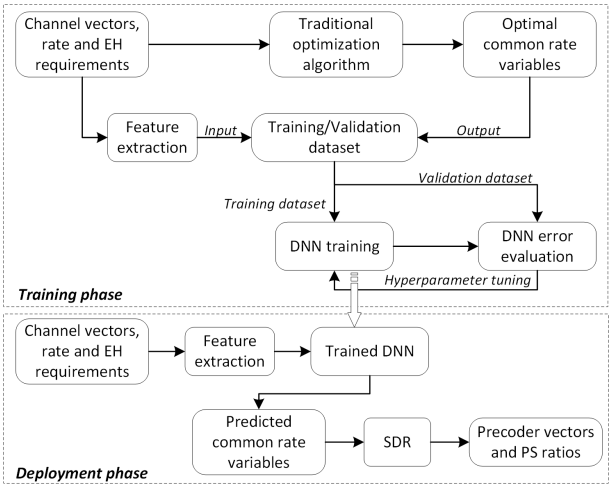

FIGURE 5. Overview of the training and deployment phases.

in Fig. 3. The input of the DNN corresponds to the encoded representation of the channel vectors given by the autoencoder, i.e. $\{\mathbf{AE}_{\mathbf{h}_1}, \ldots, \mathbf{AE}_{\mathbf{h}_U}, \mathbf{AE}_{\mathbf{q}_1}, \ldots, \mathbf{AE}_{\mathbf{g}_K}\}$, and the rate and energy requirements of the hybrid and ID users. The output of the DNN module is the common rate variables $\left\{r^H_{u,c}, r^{ID}_{d,c}\right\}$. The DNN module solves a regression problem in order to map the input of the DNN to the common rate variables. Thus, a dataset with the optimal common rate for each input is required to train the DNN by optimizing the weights of the network.

Fig. 5 illustrates the overview process for the training and deployment phases. First, the training and validation datasets are collected based on the solution of traditional optimization algorithms and features extracted from the channel vectors, and rate and EH requirements. The feature extraction is performed by the autoencoder module in Fig. 4. We considered the PSO–SDR solution from [30] as the traditional optimization algorithm to solve the minimum transmit power problem in the proposed scheme. However, PSO–SDR is an iterative algorithm that requires solving an SDR problem dozens of times, which involves high computational complexity. Therefore, in this paper, we approximate the PSO algorithm with the DNN module deployed at the STx. Next, the training dataset is used to optimize the weights of the DNN, and the validation data is used to select the best hyperparameters of the DNN. Finally, the trained DNN is used for the deployment phase detailed in Fig. 3.

An additional step after the DNN module is the filtering process, which limits the values for the common rate variables. These limits are obtained based on the problem formulation and their related constraints, as follows. We denote the maximum values for $r^H_{u,c}$ and $r^{ID}_{d,c}$ as $r^H_{u,max}$ and $r^{ID}_{d,max}$, respectively. Based on constraint (10d), we derive the following:

$$r^H_{u,\max_1} = \min_{1\le i\le U}\left\{\log_2\left(1+\frac{\left|\mathbf{h}_i^H\mathbf{w}_{c\max}\right|^2}{\sigma^2_{H,i}+\gamma_i^2}\right)\right\}. \quad (12)$$

Then, by using the Cauchy–Schwarz inequality and limiting the norm of precoder vector $\mathbf{w}_c$ to $P_{\max}$, (12) becomes

$$r^H_{u,\max_1} \le \min_{1\le i\le U}\left\{\log_2\left(1+\frac{\|\mathbf{h}_i\|^2 P_{\max}}{\sigma^2_{H,i}+\gamma_i^2}\right)\right\}. \quad (13)$$

By following the procedures in (12) and (13), and based on constraint (10e), an additional limit for $r^H_{u,max}$ is defined as follows:

$$r^H_{u,\max_2} \le \min_{1\le j\le D}\left\{\log_2\left(1+\frac{\|\mathbf{q}_j\|^2 P_{\max}}{\sigma^2_{ID,j}}\right)\right\}, \quad (14)$$

where we denote $\delta_1 = \min_{1\le i\le U}\left\{\log_2\left(1+\frac{\|\mathbf{h}_i\|^2 P_{\max}}{\sigma^2_{H,i}+\gamma_i^2}\right)\right\}$ and $\delta_2 = \min_{1\le j\le D}\left\{\log_2\left(1+\frac{\|\mathbf{q}_j\|^2 P_{\max}}{\sigma^2_{ID,j}}\right)\right\}$ for future use. In the case of $r^{ID}_{d,max}$, it can be shown that the same limits, δ_1 and δ_1, are attained by following the aforementioned process from (12) to (14).

The maximum value of $r^H_{u,c}$ is also restricted by constraints (10b) and (10d) through the terms $\beta = 2^{\sum_{i=1}^{U} r^H_{i,c} + \sum_{d=1}^{D} r^{ID}_{d,c}} - 1$ and $\alpha^H_u = \max\left\{0, 2^{R^H_{u,\min} - r^H_{u,c}} - 1\right\}$. First, we analyze the case where $r^H_{u,c} < R^H_{u,\min}$, which leads to a value of α^H_u greater than zero while restricting the value of $r^H_{u,c}$ to $\left[0, R^H_{u,\min}\right)$. Second, we consider the case where $r^H_{u,c} \ge R^H_{u,\min}$, which leads to a value of zero for α^H_u. In this case, we notice that constraint (10b) is always satisfied for all possible values of $\mathbf{w}_c, \{\mathbf{w}_u, \mathbf{v}_d, \rho_u\}$. Then, we use constraint (10d) to limit the maximum value of $r^H_{u,c}$ to $R^H_{u,\min}$. This is because, as we reduce the value of β, by decreasing $r^H_{u,c}$, a lower value of $\left|\mathbf{h}_u^H\mathbf{w}_c\right|^2$ is required while reducing the transmission power. Therefore, we can conclude that another limit for the maximum value of $r^H_{u,c}$ is $R^H_{u,\min}$.

For $r^{ID}_{d,max}$, by following the previous procedure and taking into account the expressions β and α^{ID}_d, and constraints (10c) and (10d), we can define $R^{ID}_{d,\min}$ as another limit on the maximum value of $r^{ID}_{d,c}$.

By combining the above results, the maximum values of the common rates are defined as

$$r^H_{u,\max} = \min\left(R^H_{u,\min}, \delta_1, \delta_2\right) \quad (15a)$$

$$r^{ID}_{d,\max} = \min\left(R^{ID}_{d,\min}, \delta_1, \delta_2\right). \quad (15b)$$

Finally, the corrected values of the common rate variables are defined as follows:

$$r^H_{u,c} = \begin{cases} 0, & \text{if } r^H_{u,c} < 0, \ \forall u, \quad (16a)\\ r^H_{u,\max}, & \text{if } r^H_{u,c} > r^H_{u,\max}, \ \forall u, \quad (16b)\\ r^H_{u,c}, & otherwise, \ \forall u \quad (16c)\end{cases}$$

$$r^{ID}_{d,c} = \begin{cases} 0, & \text{if } r^{ID}_{d,c} < 0, \ \forall d, \quad (17a)\\ r^{ID}_{d,\max}, & \text{if } r^{ID}_{d,c} > r^{ID}_{d,\max}, \ \forall d, \quad (17b)\\ r^{ID}_{d,c}, & otherwise, \ \forall d \quad (17c)\end{cases}$$

For the DNN module, we consider the computational complexity of the online prediction because the training process is performed in offline. The complexity of the DNN module depends on the number of layers and nodes. We have $J\left(U+D+K\right)+2U+D$ nodes in the input layer, $U+D$ nodes in the output layer and m_i^{DNN} nodes in the i-th hidden layer where $i=1,\ldots,M_{DNN}$. Then, the computational complexity of the DNN module is given by $\mathcal{O}\left(\left(J\left(U+D+K\right)+2U+D\right)m_1^{DNN}+m_1^{DNN}m_2^{DNN}+\ldots+m_{M_{DNN}}^{DNN}\left(U+D\right)\right)$, which can be approximated by $\mathcal{O}\left(J\left(U+D+K\right)\right)$ when parameters of the DNN are assumed to be fixed.

One substantial advantage of the autoencoder module is the ability to adapt the proposed approach to several numbers of transmitting antennas while keeping the same DNN module. In particular, collecting data and training an autoencoder is a relatively easy job, since it is an unsupervised method. Then, we can train a new autoencoder module when the number of antennas at the STx increases, while keeping the same dimensions in the middle layer (J units) so that we can use the same DNN module for several numbers of transmitting antennas. We analyze this capability in the simulation results of Section IV.B. Note that training a new DNN (without the autoencoder module) for a different number of transmitting antennas requires collecting new datasets, which is a time-consuming task since the DNN module needs the optimal common rate variables as output for each input sample in order to optimize the weights.

The third module is the SDR-based approach, which is used to solve problem (10) where a penalty-based method is applied to guarantee a feasible solution.

C. SDR-BASED APPROACH TO SOLVING PROBLEM (10)

We propose using the SDR technique [38] to solve minimum transmit power problem (10). First, we define $\mathbf{W}_c=\mathbf{w}_c\mathbf{w}_c^H$, $\mathbf{W}_u=\mathbf{w}_u\mathbf{w}_u^H$, $\mathbf{V}_d=\mathbf{v}_d\mathbf{v}_d^H$, $\mathbf{H}_u=\mathbf{h}_u\mathbf{h}_u^H$, $\mathbf{Q}_d=\mathbf{q}_d\mathbf{q}_d^H$, and $\mathbf{G}_k=\mathbf{g}_k\mathbf{g}_k^H$. Then, it follows that $\mathbf{W}_c$, $\mathbf{W}_u$ and $\mathbf{V}_d$ are rank-one symmetric positive semidefinite matrices, i.e. $\mathbf{W}_c,\mathbf{W}_u,\mathbf{V}_d\succeq 0$, $\mathrm{rank}\left(\mathbf{W}_c\right)=1$, $\mathrm{rank}\left(\mathbf{W}_u\right)=1$, and $\mathrm{rank}\left(\mathbf{V}_d\right)=1$. Moreover, we have the following equivalences: $\|\mathbf{w}_c\|^2=\mathrm{Tr}\left(\mathbf{W}_c\right)$, $\|\mathbf{w}_u\|^2=\mathrm{Tr}\left(\mathbf{W}_u\right)$, $\|\mathbf{v}_d\|^2=\mathrm{Tr}\left(\mathbf{V}_d\right)$, $\left|\mathbf{h}_u^H\mathbf{w}_u\right|^2=\mathrm{Tr}(\mathbf{H}_u\mathbf{W}_u)$, and $\left|\mathbf{q}_d^H\mathbf{v}_d\right|^2=\mathrm{Tr}(\mathbf{Q}_d\mathbf{V}_d)$. Then, by ignoring the rank-one constraints for matrices $\mathbf{W}_c$, $\mathbf{W}_u$ and $\mathbf{V}_d$, the original problem (10) can be converted to the following problem:

$$\min_{\mathbf{W}_c,\{\mathbf{W}_u,\mathbf{V}_d,\rho_u\}}\ \mathrm{Tr}\left(\mathbf{W}_c\right)+\sum_{u=1}^{U}\mathrm{Tr}\left(\mathbf{W}_u\right)+\sum_{d=1}^{D}\mathrm{Tr}\left(\mathbf{V}_d\right) \quad (18a)$$

subject to:

$$-\mathrm{Tr}\left(\mathbf{H}_u\mathbf{W}_u\right)+\sum_{i=1,i\neq u}^{U}\mathrm{Tr}\left(\mathbf{H}_u\mathbf{W}_i\right)\alpha_u^H+\sum_{d=1}^{D}\mathrm{Tr}\left(\mathbf{H}_u\mathbf{V}_d\right)\alpha_u^H+\sigma_{H,u}^2\alpha_u^H+\frac{\alpha_u^H\gamma_u^2}{\rho_u}\leq 0,\ \forall u \quad (18b)$$

$$-\mathrm{Tr}\left(\mathbf{Q}_d\mathbf{V}_d\right)+\sum_{u=1}^{U}\mathrm{Tr}\left(\mathbf{Q}_d\mathbf{W}_u\right)\alpha_d^{ID}+\sum_{j=1,j\neq d}^{D}\mathrm{Tr}\left(\mathbf{Q}_d\mathbf{V}_j\right)\alpha_d^{ID}+\sigma_{ID,d}^2\alpha_d^{ID}\leq 0,\ \forall d \quad (18c)$$

$$\frac{-\mathrm{Tr}\left(\mathbf{H}_u\mathbf{W}_c\right)}{\beta}+\sum_{i=1}^{U}\mathrm{Tr}\left(\mathbf{H}_u\mathbf{W}_i\right)+\sum_{d=1}^{D}\mathrm{Tr}\left(\mathbf{H}_u\mathbf{V}_d\right)+\sigma_{H,u}^2+\frac{\gamma_u^2}{\rho_u}\leq 0,\ \forall u \quad (18d)$$

$$\frac{-\mathrm{Tr}\left(\mathbf{Q}_d\mathbf{W}_c\right)}{\beta}+\sum_{u=1}^{U}\mathrm{Tr}\left(\mathbf{Q}_d\mathbf{W}_u\right)+\sum_{j=1}^{D}\mathrm{Tr}\left(\mathbf{Q}_d\mathbf{V}_j\right)+\sigma_{ID,d}^2\leq 0,\ \forall d \quad (18e)$$

$$-\mathrm{Tr}\left(\mathbf{H}_u\mathbf{W}_c\right)-\sum_{i=1}^{U}\mathrm{Tr}\left(\mathbf{H}_u\mathbf{W}_i\right)-\sum_{d=1}^{D}\mathrm{Tr}\left(\mathbf{H}_u\mathbf{V}_d\right)-\sigma_{H,u}^2+\frac{\psi_u}{\eta_u\left(1-\rho_u\right)}\leq 0,\ \forall u \quad (18f)$$

$$\mathrm{Tr}\left(\mathbf{W}_c\right)+\sum_{u=1}^{U}\mathrm{Tr}\left(\mathbf{W}_u\right)+\sum_{d=1}^{D}\mathrm{Tr}\left(\mathbf{V}_d\right)\leq P_{\max} \quad (18g)$$

$$\mathrm{Tr}\left(\mathbf{G}_k\mathbf{W}_c\right)+\sum_{u=1}^{U}\mathrm{Tr}\left(\mathbf{G}_k\mathbf{W}_u\right)+\sum_{d=1}^{D}\mathrm{Tr}\left(\mathbf{G}_k\mathbf{V}_d\right)-\chi_k\leq 0,\ \forall k \quad (18h)$$

$$0<\rho_u<1,\ \forall u \quad (18i)$$

$$\mathbf{W}_c,\mathbf{W}_u,\mathbf{V}_d\succeq 0,\ \forall u,\ \forall d. \quad (18j)$$

Problem (18) is convex, and the convex optimization toolbox CVX [39] in Matlab can be used to obtain the solution. In constraints (18b), (18d), and (18f), note that the expressions $\frac{\gamma_u^2}{\rho_u}$ and $\frac{\psi_u}{\eta_u(1-\rho_u)}$ are convex functions with respect to ρ_u with $0<\rho_u<1$. Problem (18) consists of $\mathrm{M}_V=U+D+1$ matrices as variables with size $N\times N$, and $L=3U+2D+K+1$ linear constraint variables. Then, the complexity for solving problem (18) is $\mathcal{O}\left(\sqrt{M_VN}\left(M_V^3N^6+M_VLN^2\right)\log\left(1/\varepsilon\right)\right)$ with a solution accuracy of $\varepsilon>0$ [18], [29]. The CVX toolbox commonly uses the interior point method to solve semidefinite programming (SDP) problems, where the convergence analysis of the interior-point algorithm can be found in Section 11 of [40].

Define $\mathbf{W}_c^*$, $\mathbf{W}_u^*$, and $\mathbf{V}_d^*$ as the optimal solutions to problem (18). Then, if $\mathbf{W}_c^*$, $\mathbf{W}_u^*$, and $\mathbf{V}_d^*$ are rank-one, the precoder vectors can be obtained by

$$\mathbf{w}_c=\sqrt{\lambda_{\max}\left(\mathbf{W}_c\right)}\kappa_{\max,W_c} \quad (19a)$$

$$\mathbf{w}_u=\sqrt{\lambda_{\max}\left(\mathbf{W}_u\right)}\kappa_{\max,W_u},\ \forall u \quad (19b)$$

$$\mathbf{v}_d=\sqrt{\lambda_{\max}\left(\mathbf{V}_d\right)}\kappa_{\max,V_u},\ \forall d, \quad (19c)$$

where $\lambda_{\max}\left(\mathbf{W}\right)$ represents the maximum eigenvalue for $\mathbf{W}$, and $\kappa_{\max,W}$ is the eigenvector corresponding to the maximum eigenvalue of $\mathbf{W}$.

Otherwise, if the rank of $\mathbf{W}_c^*$, $\mathbf{W}_u^*$, and $\mathbf{V}_d^*$ is larger than rank-one, we can apply the Gaussian randomization method or the penalty function method [5], [41], [42]. The Gaussian randomization method [29], [38] consists of creating a set of candidate precoder vectors to achieve a near-optimal solution based on the eigen-decomposition of precoder matrices $\mathbf{W}_c^*$, $\mathbf{W}_u^*$, and $\mathbf{V}_d^*$ and random Gaussian vectors. However, the Gaussian randomization method cannot guarantee feasible solutions within the set of candidate precoder vectors. Note that in the proposed approach, the common rate variables are obtained based on a DNN method, which gives approximate optimal solutions. Then, the SDR module needs to provide precoder vectors that guarantee a feasible solution.

In [41], the authors proposed a penalty function method that consists of finding a close optimal solution by approximating rank-one matrices. Since $\mathbf{W}_u$ is positive semidefinite, with all its eigenvalues being non-negative, it is true that $\mathrm{Tr}(\mathbf{W}_u) \geq \lambda_{\max}(\mathbf{W}_u)$, where $\lambda_{\max}(\mathbf{W}_u)$ represents the maximum eigenvalue of $\mathbf{W}_u$. If $\mathbf{W}_u$ is rank-one, the equality is true, i.e. $\mathrm{Tr}(\mathbf{W}_u) = \lambda_{\max}(\mathbf{W}_u)$. The aforementioned analysis is also applied to matrices $\mathbf{W}_c$ and $\mathbf{V}_d$. Therefore, our objective is to make $\mathrm{Tr}(\mathbf{W}_u) - \lambda_{\max}(\mathbf{W}_u)$ as small as possible. To achieve this goal, we include penalty terms in the objective function, as follows:

$$\begin{aligned}\min_{\mathbf{W}_c,\{\mathbf{W}_u,\mathbf{V}_d,\rho_u\}} \quad & \mathrm{Tr}(\mathbf{W}_c) + \sum_{u=1}^{U}\mathrm{Tr}(\mathbf{W}_u) + \sum_{d=1}^{D}\mathrm{Tr}(\mathbf{V}_d) \\ & + \phi\left(\mathrm{Tr}(\mathbf{W}_c) - \lambda_{\max}(\mathbf{W}_c)\right) \\ & + \phi\sum_{u=1}^{U}\left(\mathrm{Tr}(\mathbf{W}_u) - \lambda_{\max}(\mathbf{W}_u)\right) \\ & + \phi\sum_{d=1}^{D}\left(\mathrm{Tr}(\mathbf{V}_d) - \lambda_{\max}(\mathbf{V}_d)\right) \qquad (20a)\end{aligned}$$

$$\text{subject to: (18b), ..., (18j),} \qquad (20b)$$

where ϕ is the penalty factor. In [41], it was established that $\lambda_{\max}(\mathbf{W}_u)$ is a convex function, so $\mathrm{Tr}(\mathbf{W}_u) - \lambda_{\max}(\mathbf{W}_u)$ is a concave function. Then, an iterative-based algorithm is proposed to find the approximate optimal solution. From [41], we have the following inequality for any $\mathbf{X}_u \succeq 0$:

$$\lambda_{\max}(\mathbf{W}_u) \geq \lambda_{\max}(\mathbf{X}_u) + \kappa_{\max,X_u}^H(\mathbf{W}_u - \mathbf{X}_u)\kappa_{\max,X_u}, \quad (21)$$

where $\kappa_{\max,X_u}$ is the unit-norm eigenvector corresponding to the maximum eigenvalue of $\mathbf{X}_u$.

Therefore, based on a given feasible $\left(\mathbf{W}_u^{(i)}\right)$ for problem (20), we can express $\lambda_{\max}(\mathbf{W}_u)$ in iteration i as follows:

$$\lambda_{\max}(\mathbf{W}_u) \geq \lambda_{\max}\left(\mathbf{W}_u^{(i)}\right) + \kappa_{\max,w_u}^{(i)H}\left(\mathbf{W}_u - \mathbf{W}_u^{(i)}\right)\kappa_{\max,w_u}^{(i)}. \quad (22)$$

Finally, we reformulate problem (20) as follows:

$$\begin{aligned}\min_{\mathbf{W}_c,\{\mathbf{W}_u,\mathbf{V}_d,\rho_u\}} \quad & \mathrm{Tr}(\mathbf{W}_c) + \sum_{u=1}^{U}\mathrm{Tr}(\mathbf{W}_u) + \sum_{d=1}^{D}\mathrm{Tr}(\mathbf{V}_d) \\ & + \phi\left(\mathrm{Tr}(\mathbf{W}_c) - \lambda_{\max}\left(\mathbf{W}_c^{(i)}\right)\right. \\ & \qquad \left. - \kappa_{\max,w_c}^{(i)H}\left(\mathbf{W}_c - \mathbf{W}_c^{(i)}\right)\kappa_{\max,w_c}^{(i)}\right) \\ & + \phi\sum_{u=1}^{U}\left(\mathrm{Tr}(\mathbf{W}_u) - \lambda_{\max}\left(\mathbf{W}_u^{(i)}\right)\right. \\ & \qquad \left. - \kappa_{\max,w_u}^{(i)H}\left(\mathbf{W}_u - \mathbf{W}_u^{(i)}\right)\kappa_{\max,w_u}^{(i)}\right) \\ & + \phi\sum_{d=1}^{D}\left(\mathrm{Tr}(\mathbf{V}_d) - \lambda_{\max}\left(\mathbf{V}_d^{(i)}\right)\right. \\ & \qquad \left. - \kappa_{\max,v_d}^{(i)H}\left(\mathbf{V}_d - \mathbf{V}_d^{(i)}\right)\kappa_{\max,v_d}^{(i)}\right) \qquad (23a)\end{aligned}$$

$$\text{subject to: (18b), ..., (18j).} \qquad (23b)$$

TABLE 1. The proposed penalty method based on problem (23) to solve problem (10).

1: **inputs:** channel vectors $\mathbf{h}_u$, $\mathbf{q}_d$, $\mathbf{g}_k$, required rate at the users $R_{u,\min}^H$, $R_{d,\min}^{ID}$, the rate of the common parts of the messages, $\left\{r_{u,c}^H, r_{d,c}^{ID}\right\}$, obtained from the DNN module, the required minimum EH at the hybrid users, ψ_u, and the approximation accuracy, $\varsigma > 0$.
2: Solve problem (18) with the CVX toolbox to obtain $\mathbf{W}_c^*$, $\left\{\mathbf{W}_u^*, \mathbf{V}_d^*, \rho_u^*\right\}$.
3: If the matrices $\mathbf{W}_c^*$, $\left\{\mathbf{W}_u^*, \mathbf{V}_d^*\right\}$ are rank-one, then use (19a)-(19c) to find precoder vectors $\mathbf{w}_c^*$, $\left\{\mathbf{w}_u^*, \mathbf{v}_d^*\right\}$, and go to step 12. Otherwise, go to step 4.
4: Initialize index $i = 0$.
5: Set the initial feasible matrices as $\mathbf{W}_c^{(i)} = \mathbf{W}_c^*$, $\mathbf{W}_u^{(i)} = \mathbf{W}_u^*$, and $\mathbf{V}_d^{(i)} = \mathbf{V}_d^*$.
6: **repeat**
7: Solve problem (23) with CVX to obtain $\mathbf{W}_c^*$, $\left\{\mathbf{W}_u^*, \mathbf{V}_d^*, \rho_u^*\right\}$.
8: Set $i = i + 1$
9: Assign the feasible points for the next iteration $\mathbf{W}_c^{(i)} = \mathbf{W}_c^*$, $\mathbf{W}_u^{(i)} = \mathbf{W}_u^*$ and $\mathbf{V}_d^{(i)} = \mathbf{V}_d^*$.
10: **until** $\left(\mathrm{Tr}\left(\mathbf{W}_c^{(i)}\right) - \lambda_{\max}\left(\mathbf{W}_c^{(i)}\right)\right) + \sum_{u=1}^{U}\left(\mathrm{Tr}\left(\mathbf{W}_u^{(i)}\right) - \lambda_{\max}\left(\mathbf{W}_u^{(i)}\right)\right) + \sum_{d=1}^{D}\left(\mathrm{Tr}\left(\mathbf{V}_d^{(i)}\right) - \lambda_{\max}\left(\mathbf{V}_d^{(i)}\right)\right) > \varsigma$
11: Use (19a)-(19c) to find the precoder vectors $\mathbf{w}_c^*$, $\left\{\mathbf{w}_u^*, \mathbf{v}_d^*\right\}$ based on $\mathbf{W}_c^{(i)}$, $\left\{\mathbf{W}_u^{(i)}, \mathbf{V}_d^{(i)}\right\}$.
12: **outputs:** $\mathbf{w}_c^*$, $\left\{\mathbf{w}_u^*, \mathbf{v}_d^*, \rho_u^*\right\}$.

Problem (23) is convex and can be solved iteratively with the CVX toolbox. The overall procedure to solve original problem (10) with the penalty method in problem (23) is described in Table 1. The precoder vector can be obtained from the matrix variables by using (19a)-(19c).

The feasibility of the problem (9) can be determined by the solution of the following optimization problem:

$$\begin{aligned}&\text{find} \quad \mathbf{w}_c, \left\{\mathbf{w}_u, \mathbf{v}_d, r_{u,c}^H, r_{d,c}^{ID}, \rho_u\right\} \qquad (24a)\\ &\text{s.t.} \quad \text{(9b), (9c), (9d), (9e), (9f), (9g), (9h), (9i), (9j)} \qquad (24b)\end{aligned}$$

The solution to problem (24) is obtained by following the procedure described in Subsection III.A for the optimization problem (9). In this paper, we focus on defining the maximum allowed values for the rate and EH requirements. First, we derive the maximum allowed value for the rate requirements at the u-th hybrid user and the d-th ID user based on the Cauchy–Schwarz inequality and the

constraints (9b), (9c), (9g), (13) and (14) as follows:

$$R^{H}_{u,\min} \leq \min(\delta_1, \delta_2) + \log_2\left(1 + \frac{\|\mathbf{h}_u\|^2 P_{\max}}{\sigma^2_{H,u}+\gamma^2_u}\right), \ \forall u \quad (25a)$$

$$R^{ID}_{d,\min} \leq \min(\delta_1, \delta_2) + \log_2\left(1 + \frac{\|\mathbf{q}_d\|^2 P_{\max}}{\sigma^2_{ID,d}}\right), \ \forall d. \quad (25b)$$

The maximum allowed value for the EH at the u-th hybrid user is derived based on (9f) and (9g) as follows:

$$\psi_u \leq \eta_u\left(\|\mathbf{h}_u\|^2 P_{\max} + \sigma^2_{H,u}\right), \quad \forall u. \quad (26)$$

Consequently, the problem (9) is infeasible if the conditions (25a), (25b), and (26) are not fulfilled. However, the feasibility of problem (9) cannot be guaranteed by only satisfying the conditions (25a), (25b), and (26). An extensive analysis of the feasibility conditions is beyond the scope of this paper and will be studied in future works.

D. ROBUST PRECODING DESIGN FOR PROBLEM (10)

In previous subsections, we assumed a perfect CSIT. However, practical systems are subject to channel estimation errors and quantization errors [14] leading to an imperfect CSI knowledge. Therefore, in this subsection, we propose a robust precoding design to deal with the imperfect CSIT based on the bounded CSI error model as follows [14] and [15]:

$$\mathcal{H}_u = \left\{\hat{\mathbf{h}}_u + \Delta\mathbf{h}_u \,\middle|\, \Delta\mathbf{h}_u^H \Delta\mathbf{h}_u \leq \varepsilon^2_{\mathbf{h},u}\right\}, \ \forall u, \quad (27a)$$

$$\mathcal{Q}_d = \left\{\hat{\mathbf{q}}_d + \Delta\mathbf{q}_d \,\middle|\, \Delta\mathbf{q}_d^H \Delta\mathbf{q}_d \leq \varepsilon^2_{\mathbf{q},d}\right\}, \ \forall d, \quad (27b)$$

$$\mathcal{G}_k = \left\{\hat{\mathbf{g}}_k + \Delta\mathbf{g}_k \,\middle|\, \Delta\mathbf{g}_k^H \Delta\mathbf{g}_k \leq \varepsilon^2_{\mathbf{g},k}\right\}, \ \forall k, \quad (27c)$$

where $\hat{\mathbf{h}}_u$, $\hat{\mathbf{q}}_d$, $\hat{\mathbf{g}}_k$ are the estimates of channel vectors, $\Delta\mathbf{h}_u$, $\Delta\mathbf{q}_d$, $\Delta\mathbf{g}_k$ are the channel uncertainty of the channel vectors $\mathbf{h}_u$, $\mathbf{q}_d$, $\mathbf{g}_k$, respectively. Moreover, $\varepsilon_{\mathbf{h},u}$, $\varepsilon_{\mathbf{q},d}$, $\varepsilon_{\mathbf{g},k}$ represent the radius of the uncertainty region for the corresponding CSI of the channels $\mathbf{h}_u$, $\mathbf{q}_d$, $\mathbf{g}_k$, respectively. Then, the robust optimization problem is composed of infinitely many constraints due to the imperfect CSI. To solve this problem, we propose the S-procedure [16], which permits dealing with the infinite number of constraints by adding extra variables while obtaining an equivalent problem with a finite number of constraints as follows.

Lemma 1 (S-procedure [16], [15]): Let $f_i(\mathbf{x}) = \mathbf{x}^H\mathbf{A}_i\mathbf{x} + 2\mathrm{Re}\{\mathbf{b}_i^H x\} + c_i$, $i = 1, 2$, where $\mathbf{A}_i = \mathbf{A}_i^H$. The condition $f_1(\mathbf{x}) \leq 0 \Rightarrow f_0(\mathbf{x}) \leq 0$ holds if, and only if, $\tau \geq 0$ such that

$$\tau\begin{bmatrix}\mathbf{A}_1 & \mathbf{b}_1\\ \mathbf{b}_1^H & c_1\end{bmatrix} - \begin{bmatrix}\mathbf{A}_2 & \mathbf{b}_2\\ \mathbf{b}_2^H & c_2\end{bmatrix} \succeq 0. \quad (28)$$

Next, we replace $\mathbf{h}_u = \hat{\mathbf{h}}_u + \Delta\mathbf{h}_u$, $\mathbf{h}_u \in \mathcal{H}_u$ into the rate constraint (10b) and reformulate the constraint as follows:

$$\Delta\mathbf{h}_u^H\mathbf{B}_u\Delta\mathbf{h}_u + 2\mathrm{Re}\left\{\left(\mathbf{B}_u\hat{\mathbf{h}}_u\right)^H\Delta\mathbf{h}_u\right\} + \hat{\mathbf{h}}_u^H\mathbf{B}_u\hat{\mathbf{h}}_u + \sigma^2_{H,u} + \frac{\gamma^2_u}{\rho_u} \leq 0, \ \Delta\mathbf{h}_u^H\Delta\mathbf{h}_u \leq \varepsilon^2_{\mathbf{h},u}, \ \forall u, \quad (29)$$

where $\mathbf{B}_u = -\frac{\mathbf{W}_u}{\alpha_u^H} + \sum_{i=1,i\neq u}^{U}\mathbf{W}_i + \sum_{d=1}^{D}\mathbf{V}_d$. Then, we deal with the CSI uncertainties in (29) based on Lemma 1 as follows: $\mathbf{x} = \Delta\mathbf{h}_u$, $\mathbf{A}_1 = \mathbf{I}_N$, $c_1 = -\varepsilon^2_{\mathbf{h},u}$, $\mathbf{A}_2 = \mathbf{B}_u$, $\mathbf{b}_2 = \mathbf{B}_u\hat{\mathbf{h}}_u$, and $c_2 = \hat{\mathbf{h}}_u^H\mathbf{B}_u\hat{\mathbf{h}}_u + \sigma^2_{H,u} + \frac{\gamma^2_u}{\rho_u} \leq 0$. Therefore, constraint (29) is rewritten as

$$\begin{bmatrix}\tau_{H,u}I_N - \mathbf{B}_u & -\mathbf{B}_u\hat{\mathbf{h}}_u\\ -\hat{\mathbf{h}}_u^H\mathbf{B}_u & -\hat{\mathbf{h}}_u^H\mathbf{B}_u\hat{\mathbf{h}}_u - \sigma^2_{H,u} - \frac{\gamma^2_u}{\rho_u} - \tau_{H,u}\varepsilon^2_{\mathbf{h},u}\end{bmatrix} \succeq 0, \ \forall u, \quad (30)$$

where $\tau_H = \left[\tau_{H,1}, \ldots, \tau_{H,U}\right]^T$ are slack variables. Similarly, we use the Lemma 1 and replace (27b) to transform the constraint (10c) as follows:

$$\begin{bmatrix}\tau_{ID,d}I_N - \mathbf{C}_d & -\mathbf{C}_d\hat{\mathbf{q}}_d\\ -\hat{\mathbf{q}}_d^H\mathbf{C}_d & -\hat{\mathbf{q}}_d^H\mathbf{C}_d\hat{\mathbf{q}}_d - \sigma^2_{ID,d} - \tau_{ID,d}\varepsilon^2_{\mathbf{q},d}\end{bmatrix} \succeq 0, \ \forall d, \quad (31)$$

where $\mathbf{C}_d = -\frac{\mathbf{V}_d}{\alpha_d^{ID}} + \sum_{u=1}^{U}\mathbf{W}_u + \sum_{j=1,j\neq d}^{D}\mathbf{V}_j$, and $\tau_{ID} = \left[\tau_{ID,1}, \ldots, \tau_{ID,D}\right]^T$ are slack variables. Next, Lemma 1 and (27a) are used to represent the constrain (10d) as follows:

$$\begin{bmatrix}\tau_{Hc,u}I_N - \mathbf{B}_c & -\mathbf{B}_c\hat{\mathbf{h}}_u\\ -\hat{\mathbf{h}}_u^H\mathbf{B}_c & -\hat{\mathbf{h}}_u^H\mathbf{B}_c\hat{\mathbf{h}}_u - \sigma^2_{H,u} - \frac{\gamma^2_u}{\rho_u} - \tau_{Hc,u}\varepsilon^2_{\mathbf{h},u}\end{bmatrix} \succeq 0, \ \forall u, \quad (32)$$

where $\mathbf{B}_c = -\frac{\mathbf{W}_c}{\beta} + \sum_{i=1}^{U}\mathbf{W}_i + \sum_{j=1}^{D}\mathbf{V}_j$, and $\tau_{Hc} = \left[\tau_{Hc,1}, \ldots, \tau_{Hc,U}\right]^T$ are slack variables. Similarly, we can use Lemma 1 and replace (27b) to transform the constraint (10e) as follows:

$$\begin{bmatrix}\tau_{IDc,d}I_N - \mathbf{B}_c & -\mathbf{B}_c\hat{\mathbf{q}}_d\\ -\hat{\mathbf{q}}_d^H\mathbf{B}_c & -\hat{\mathbf{q}}_d^H\mathbf{B}_c\hat{\mathbf{q}}_d - \sigma^2_{ID,d} - \tau_{IDc,d}\varepsilon^2_{\mathbf{q},d}\end{bmatrix} \succeq 0, \ \forall d, \quad (33)$$

where $\tau_{IDc} = \left[\tau_{IDc,1}, \ldots, \tau_{IDc,D}\right]^T$ are slack variables.

The EH constraint (9f) can be reformulated with Lemma 1 and (27a) as follows:

$$\begin{bmatrix}\tau_{E,u}I_N - \mathbf{E} & -\mathbf{E}\hat{\mathbf{h}}_u\\ -\hat{\mathbf{h}}_u^H\mathbf{E} & -\hat{\mathbf{h}}_u^H\mathbf{E}\hat{\mathbf{h}}_u + \sigma^2_{H,u} - \frac{\psi_u}{\eta_u(1-\rho_u)} - \tau_{E,u}\varepsilon^2_{\mathbf{h},u}\end{bmatrix} \succeq 0, \ \forall u, \quad (34)$$

where $\mathbf{E} = -\mathbf{W}_c - \sum_{i=1}^{U}\mathbf{W}_i - \sum_{j=1}^{D}\mathbf{V}_j$, and $\tau_E = \left[\tau_{E,1}, \ldots, \tau_{E,U}\right]^T$ are slack variables. Finally, the interference power constraint (9h) is reformulated with (27c) and Lemma 1 into the following:

$$\begin{bmatrix}\tau_{PU,k}I_N + \mathbf{E} & \mathbf{E}\hat{\mathbf{g}}_k\\ \hat{\mathbf{g}}_k^H\mathbf{E} & \hat{\mathbf{g}}_k^H\mathbf{E}\hat{\mathbf{g}}_k + \chi_k - \tau_{PU,k}\varepsilon^2_{\mathbf{g},k}\end{bmatrix} \succeq 0, \ \forall k, \quad (35)$$

where $\tau_{PU} = \left[\tau_{PU,1}, \ldots, \tau_{PU,K}\right]^T$ are slack variables.

Based on [15], we propose the variables υ_u and $\tilde{\upsilon}_u$ to replace $\frac{1}{\rho_u}$ and $\frac{1}{1-\rho_u}$ in (30), (32), and (34). Therefore, by ignoring the rank-one constraint, the optimization problem in (10) under imperfect CSIT can be formulated as follows

$$\min_{\left\{\begin{array}{c}\mathbf{W}_c, \mathbf{W}_u, \mathbf{V}_d, \rho_u, \\ \upsilon_u, \tilde{\upsilon}_u, \tau_{H,u}, \tau_{ID,d}, \\ \tau_{Hc,u}, \tau_{IDc,d}, \tau_{E,u}, \\ \tau_{PU,k}\end{array}\right\}} Tr\left(\mathbf{W}_c\right)+\sum_{u=1}^{U} Tr\left(\mathbf{W}_u\right)+\sum_{d=1}^{D} Tr\left(\mathbf{V}_d\right) \tag{36a}$$

$$\text{s.t. (30), (31), (32), (33), (34) and (35)} \tag{36b}$$

$$\upsilon_u \geq \frac{1}{\rho_u},\ \tilde{\upsilon}_u \geq \frac{1}{1-\rho_u},\ \forall u \tag{36c}$$

$$\tau_{H,u}, \tau_{ID,d}, \tau_{Hc,u}, \tau_{IDc,d}, \tau_{E,u}, \tau_{PU,k} \geq 0,\ \forall u,\ \forall d,\ \forall k \tag{36d}$$

$$\mathbf{W}_c, \mathbf{W}_u, \mathbf{V}_d \succeq 0,\ \forall u,\ \forall d \tag{36e}$$

$$0 < \rho_u < 1,\ \forall u. \tag{36f}$$

Problem (36) is convex and can be solved with the CVX toolbox in MATLAB. Moreover, if the matrix solutions are not rank-one, the penalty method of Subsection III.C is used to obtain the solution of the beamforming vectors. The complexity of the problem (36) can be given by $\mathcal{O}\left(\sqrt{A_R M_s + B_R N} \cdot z_o \cdot \left[z_o^2 + A_R M_s^3 + B_R N^3 + z_o\left(A_R M_s^2 + B_R N^2\right)\right]\right) \log\left(\frac{1}{\xi}\right)$ because the problem (36) is composed of $A_R = 3U + 2D + K$ linear matrix inequality (LMI) constraints with size $M_s = N + 1$, $B_R = U + D + 1$ LMI constraints with size N, and the number of decision variables has an order of $z_0 = B_R N^2$ [43].

E. THE NOMA-BASED APPROACH

We describe the NOMA-based scheme [12] used as a comparative scheme for the proposed system model. We consider two groups of users, one group composed of hybrid users, and the other group composed of ID users. Then, we apply NOMA in each group while treating the interference between groups as noise. In NOMA, the original messages, m_u^H and m_d^{ID}, intended for the u-th hybrid user and the d-th ID user, are independently encoded into private streams $\tilde{s}_u^H$ and $\tilde{s}_d^{ID}$, respectively. The precoder vectors for streams $\tilde{s}_u^H$ and $\tilde{s}_d^{ID}$ are defined as $\tilde{\mathbf{w}}_u \in \mathbb{C}^{Nx1}$ and $\tilde{\mathbf{v}}_d \in \mathbb{C}^{Nx1}$, respectively. We consider the users to be ordered according to their channel strengths: $\|\mathbf{h}_1\| \geq \|\mathbf{h}_2\| \geq \ldots. \geq \|\mathbf{h}_U\|$ and $\|\mathbf{q}_1\| \geq \|\mathbf{q}_2\| \geq \ldots. \geq \|\mathbf{q}_D\|$.

The SIC procedure for the u-th hybrid user permits it to successively decode and subtract the intended signals for the weaker users, $u+1, \ldots, U$. Similarly, the signals of the weaker users, $d+1, \ldots, D$, are decoded through the SIC layers at the d-th ID user.

The achievable rate at the u-th hybrid user when decoding the signal intended for the i-th hybrid user can be expressed as

$$\mathrm{R}_{u,i}^H = \log_2\left(1 + \frac{\left|\mathbf{h}_u^H \tilde{\mathbf{w}}_i\right|^2}{\sum_{j=1}^{i-1}\left|\mathbf{h}_u^H \tilde{\mathbf{w}}_j\right|^2 + \sum_{d=1}^{D}\left|\mathbf{h}_u^H \tilde{\mathbf{v}}_d\right|^2 + \sigma_{H,u}^2 + \frac{\gamma_u^2}{\rho_u}}\right), \quad \forall u,\ \forall i \geq u. \tag{37}$$

The achievable rate at the d-th ID user when decoding the signal intended for the r-th ID user can be expressed as

$$\mathrm{R}_{d,r}^{ID} = \log_2\left(1 + \frac{\left|\mathbf{q}_d^H \tilde{\mathbf{v}}_r\right|^2}{\sum_{u=1}^{U}\left|\mathbf{q}_d^H \tilde{\mathbf{w}}_u\right|^2 + \sum_{j=1}^{r-1}\left|\mathbf{q}_d^H \tilde{\mathbf{v}}_j\right|^2 + \sigma_{ID,d}^2}\right), \quad \forall d,\ \forall r \geq d. \tag{38}$$

The energy harvested at the EH module of the u-th hybrid user is given by

$$E_{u,NOMA}^H = \eta_u\left(1-\rho_u\right)\left(\sum_{j=1}^{U}\left|\mathbf{h}_u^H \tilde{\mathbf{w}}_j\right|^2 + \sum_{d=1}^{D}\left|\mathbf{h}_u^H \tilde{\mathbf{v}}_d\right|^2 + \sigma_{H,u}^2\right), \quad \forall u. \tag{39}$$

The interference power at the k-th PU is given by

$$\mathrm{P}_{k,NOMA}^{\mathrm{int}} = \sum_{u=1}^{U}\left|\mathbf{g}_k^H \tilde{\mathbf{w}}_u\right|^2 + \sum_{d=1}^{D}\left|\mathbf{g}_k^H \tilde{\mathbf{v}}_d\right|^2,\ \forall k. \tag{40}$$

Therefore, minimization of the total transmit power at the STx by considering the NOMA method, subject to the minimum data rate requirement, the minimum EH requirement, and the maximum power allowed for interference with the PUs, is formulated as follows:

$$\min_{\{\tilde{\mathbf{w}}_u, \tilde{\mathbf{v}}_d, \rho_u\}} \sum_{u=1}^{U}\left\|\tilde{\mathbf{w}}_u\right\|^2 + \sum_{d=1}^{D}\left\|\tilde{\mathbf{v}}_d\right\|^2 \tag{41a}$$

$$\text{s.t. } R_{u,i}^H \geq R_{i,\min}^H,\ \forall u,\ \forall i \geq u \tag{41b}$$

$$R_{d,r}^{ID} \geq R_{r,\min}^{ID},\ \forall d,\ \forall r \geq d \tag{41c}$$

$$\mathrm{E}_{u,NOMA}^H \geq \psi_u,\ \forall u \tag{41d}$$

$$\sum_{u=1}^{U}\left\|\tilde{\mathbf{w}}_u\right\|^2 + \sum_{d=1}^{D}\left\|\tilde{\mathbf{v}}_d\right\|^2 \leq P_{\max} \tag{41e}$$

$$\mathrm{P}_{k,NOMA}^{\mathrm{int}} \leq \chi_k,\ \forall k \tag{41f}$$

$$0 < \rho_u < 1,\ \forall u. \tag{41g}$$

Problem (41) is non-convex and can be reformulated as a convex problem by using the SDR technique, detailed in Section III.C, as follows:

$$\min_{\left\{\tilde{\mathbf{W}}_u, \tilde{\mathbf{V}}_d, \rho_u\right\}} \sum_{u=1}^{U}\mathrm{Tr}\left(\tilde{\mathbf{W}}_u\right) + \sum_{d=1}^{D}\mathrm{Tr}\left(\tilde{\mathbf{V}}_d\right) \tag{42a}$$

Subject to:

$$-\mathrm{Tr}\left(\mathbf{H}_u\tilde{\mathbf{W}}_i\right)+\sum_{j=1}^{i-1}\mathrm{Tr}\left(\mathbf{H}_u\tilde{\mathbf{W}}_j\right)\tilde{\alpha}_i^H+\sum_{d=1}^{D}\mathrm{Tr}\left(\mathbf{H}_u\tilde{\mathbf{V}}_d\right)\tilde{\alpha}_i^H+\sigma_{H,u}^2\tilde{\alpha}_i^H+\frac{\tilde{\alpha}_i^H\gamma_u^2}{\rho_u}\leq 0,\ \ \forall u,\ \forall i\geq u \tag{42b}$$

$$-\mathrm{Tr}\left(\mathbf{Q}_d\tilde{\mathbf{V}}_r\right)+\sum_{u=1}^{U}\mathrm{Tr}\left(\mathbf{Q}_d\tilde{\mathbf{W}}_u\right)\tilde{\alpha}_r^{ID}+\sum_{j=1}^{r-1}\mathrm{Tr}\left(\mathbf{Q}_d\tilde{\mathbf{V}}_j\right)\tilde{\alpha}_r^{ID}+\sigma_{ID,d}^2\tilde{\alpha}_r^{ID}\leq 0,\ \ \forall d,\ \forall r\geq d \tag{42c}$$

$$-\sum_{j=1}^{U}\mathrm{Tr}\left(\mathbf{H}_u\tilde{\mathbf{W}}_j\right)-\sum_{d=1}^{D}\mathrm{Tr}\left(\mathbf{H}_u\tilde{\mathbf{V}}_d\right)-\sigma_{H,u}^2+\frac{\psi_u}{\eta_u\left(1-\rho_u\right)}\leq 0,\ \ \forall u \tag{42d}$$

$$\sum_{u=1}^{U}\mathrm{Tr}\left(\tilde{\mathbf{W}}_u\right)+\sum_{d=1}^{D}\mathrm{Tr}\left(\tilde{\mathbf{V}}_d\right)\leq P_{\max} \tag{42e}$$

$$\sum_{u=1}^{U}\mathrm{Tr}\left(\mathbf{G}_k\tilde{\mathbf{W}}_u\right)+\sum_{d=1}^{D}\mathrm{Tr}\left(\mathbf{G}_k\tilde{\mathbf{V}}_d\right)-\chi_k\leq 0,\ \ \forall k \tag{42f}$$

$$0<\rho_u<1,\ \ \forall u \tag{42g}$$

$$\tilde{\mathbf{W}}_u,\tilde{\mathbf{V}}_d\succeq 0,\ \ \forall u,\ \forall d \tag{42h}$$

where $\tilde{\alpha}_i^H=2^{R_{i,\min}^H}-1$, and $\tilde{\alpha}_r^{ID}=2^{R_{r,\min}^{ID}}-1$. Problem (42) is convex and can be solved with the CVX toolbox, based on the Algorithm in Table 1 using the penalty method if the rank of $\tilde{\mathbf{W}}_u^*$ and $\tilde{\mathbf{V}}_d^*$ is larger than rank-one.

F. COMPARATIVE ITERATIVE SCHEMES

The proposed DNN-based scheme is not an iterative scheme and the solution to the problem (9) consists of two steps. In the first step, the value of the common rate variables is provided as the output of the DNN module. In the second step, an SDR-based scheme is used to optimize the beamforming vectors and PS ratios. On the other hand, iterative algorithms require dozens of steps to achieve the close-optimal solution while solving an optimization problem in each step. Then, iterative algorithms have high computational complexity, which limits the use of those algorithms in practical scenarios where a fast solution is required due to the changing nature of the wireless channels.

We consider a PSO-based scheme with SDR [30] as the main comparative iterative scheme. The PSO algorithm is a metaheuristic algorithm used to obtain the value of the common rate variables and the SDR method is used to optimize the beamforming vectors and PS ratios. In particular, the PSO scheme consists of N_{PSO} particles, where each particle has a position with a dimension which is equal to the number of common rate variables. First, the positions of the N_{PSO} particles are randomly initialized within the constraints detailed in (15a) and (15b), and their corresponding objective function values are obtained from (9a) after solving the SDR-based problem (18) for each particle. Next, based on the objective function of each particle and the best particle in the swarm, the PSO algorithm evaluates the velocity of each particle which is used to update the particle's positions for the next iteration. Then, the updated particle's positions, which represent the common rate variables, are used as inputs to calculate their corresponding objective function values by solving the problem (18). The aforementioned process is repeated until convergence is being reached, which can be defined based on a maximum number of iterations $I_{PSO}^{\max}$ or a relative change in the objective function. Consequently, in each iteration, the problem (18) needs to be solved N_{PSO} times. A detailed description of the PSO algorithm can be found in [30].

For comparison purposes, we consider three additional schemes based on the metaheuristic algorithms: the genetic algorithm (GA) [44], the cuckoo search (CS) algorithm [45], and the butterfly optimization algorithm (BOA) [46]. These metaheuristic algorithms are based on an iterative approach with a similar procedure to the PSO-based scheme. That is, the metaheuristic algorithm is used to optimize the common rate variables and the SDR-based problem (18) is used to obtain the beamforming vectors and PS ratios. GA is based on a set of N_{GA} chromosomes, where each chromosome is composed of several variables representing the common rate variables. The value of the chromosomes is updated based on selection rules and mutation methods to obtain the best chromosome that minimizes the objective function in a total of $I_{GA}^{\max}$ generations. The CS algorithm consists of N_{CS} host nests with a dimension representing the common rate variables, where the variables in the nests are updated in each iteration based on the Lévy flight until reaching a maximum number of iterations $I_{CS}^{\max}$. Moreover, a portion $p_{a,CS}$ of the worst nests is discarded and will be replaced by newly generated nests in each iteration. BOA is composed of a population of N_{BOA} butterflies with a position representing the values of the common rate variables. The position of each butterfly is updated in each iteration based on the fragrance of the butterfly, determined by its fitness function, until a maximum number of generations $I_{BOA}^{\max}$ is being reached.

The complexity of the proposed DNN-SDR scheme is composed of the complexity of the DNN module described in Subsection III.B and the complexity to solve the problem (18) detailed in Subsection III.C. Then, the total complexity of the proposed DNN-SDR approach is given by $\mathcal{O}\left(\mathrm{J}\left(\mathrm{U}+\mathrm{D}+\mathrm{K}\right)+\psi_{SDR}\right)$, where $\psi_{SDR}=\mathcal{O}\left(\sqrt{M_vN}\left(M_V^3N^6+M_vLN^2\right)\right)$ represents the complexity to solve the problem (18). Note that the complexity of the proposed DNN-based scheme can be simplified to that of solving the problem (18) because the complexity of the DNN module is very low and can be omitted. Concerning the comparative iterative schemes, the PSO-based algorithm has

a complexity of $\mathcal{O}\left(N_{PSO} I_{PSO}^{\max} \psi_{SDR}\right)$. The CS-based scheme has a complexity of $\mathcal{O}\left(I_{CS}^{\max}\left(N_{CS} + p_{a,CS} N_{CS}\right)\psi_{SDR}\right)$. In the case of BOA, the complexity is given by $\mathcal{O}\left(I_{BOA}^{\max} N_{BOA} \psi_{SDR}\right)$.

The proposed DNN-based scheme does not require an initial point since the inputs are the channel vectors and rate and EH requirements. However, if the values of the common rate variables, provided as the output of DNN, leads to an infeasible solution to the problem (18), we can set these variables to zero and remove the beamforming vector $\mathbf{w}_c$ with its corresponding constraints (9d) and (9e). In this case, the RSMA-based problem is transformed into an SDMA-based problem, which does not require an initial feasible point. It is worth highlighting that in our simulations, the proposed DNN-based scheme has provided feasible values for the common rate variables in all the considered scenarios.

On the other hand, feasible starting points are required for iterative-based schemes. In particular, we only need to analyze a feasible initial value for the common rates, which are limited based on (16) and (17) as mentioned in Subsection III.B. Then, based on the analysis of (16) and (17), we can increase the possibility of selecting a feasible initial point since we limit the search area for the common rate variables. Moreover, the iterative-based schemes, used for comparison purposes in this paper, start with a population of 10 individuals where it is expected that at least one feasible point was found in the set.

IV. SIMULATION RESULTS

In this section, we present numerical results to prove the effectiveness of our proposed scheme based on a DNN with an autoencoder and the SDR technique, denoted as DNN–SDR RSMA. The values of the parameters adopted in the simulation are $N = 8$, $U = 2$, $D = 2$, $K = 2$, $\gamma_u^2 = \sigma_{H,u}^2 = \alpha_{ID,d}^2 = -60$dBm, $R_{u,\min}^H = R_{d,\min}^{ID} = R_{\min}$, $\psi_u = \psi$, $\eta_u = 1$, $\chi_k = -60$dBm, $\varsigma = 0.0001$, and $P_{\max} = 40$dBm. The simulations were performed on a computer with an Intel Core i7 and 16GB of RAM.

As mentioned in Section III.B, the DNN module is a supervised scheme that requires training data to learn the optimal parameters. Thus, we used our previously proposed solution for a MISO SWIPT cognitive radio system [30] to obtain the dataset by assuming a perfect CSIT. We compared the results of the proposed scheme with baseline schemes using SDMA and NOMA as described in Section III.E of [37] and Section III.D of this paper, respectively. Moreover, we consider the iterative schemes described in Section III.F of this paper as comparative approaches. All compared methods were implemented with the penalty method when the matrix variables were higher than rank-one.

In each example, we considered Rician fading to construct the channel vectors from the STx to the hybrid and ID users, as well as Rayleigh fading for channels to the PUs. We assumed a signal attenuation of Ω dB from the STx to the hybrid and ID users. For instance, an average distance of five meters corresponds to a signal attenuation of $\Omega = 40$ dB [9]. The channel from the STx to the u-th hybrid user is expressed as

$$\mathbf{h}_u = \sqrt{\frac{K_R}{1+K_R}}\mathbf{h}_u^{LOS} + \sqrt{\frac{1}{1+K_R}}\mathbf{h}_u^{NLOS}, \tag{43}$$

where $\mathbf{h}_u^{LOS}$ is the line-of-sight (LOS) deterministic component, K_R is the Rician factor equal to 5dB, and $\mathbf{h}_u^{NLOS}$ denotes the Rayleigh fading component composed of CSCG random variables with zero mean and covariance of $-\Omega$ dB. To generate $\mathbf{h}_u^{LOS}$, we considered the far-field uniform linear antenna array model given in [47]:

$$\mathbf{h}_u^{LOS} = 10^{-\frac{\Omega}{10}}\Big[1\, e^{-j\pi \sin\left(\theta_u^H\right)}\, e^{-j2\pi \sin\left(\theta_u^H\right)} \ldots\, e^{-j(N-1)\pi \sin\left(\theta_u^H\right)}\Big]^T, \tag{44}$$

where θ_u^H represents the direction of the u-th hybrid user to the STx, and assuming that spacing between antennas at the STx is half the carrier wavelength. To generate the channel vectors, $\mathbf{q}_d$, we used the aforementioned procedure in (43) and (44), with θ_u^{ID} being the direction of the d-th ID user to the STx. The channel vectors, $\mathbf{g}_k$ (from the STx to the PUs), were modeled with Rayleigh fading considering a power attenuation of 60dB.

We considered three separate datasets: training, validation, and testing. The training data were used to optimize the weights of the DNN module, and the validation data were used to select the best hyperparameters of the DNN, such as the learning rate, the number of hidden layers and units, the batch size, the number of epochs, and so on. The testing data were used to evaluate the performance of the final model, i.e. the model trained with the best hyperparameters. The training data is comprised of 6800 samples with a signal attenuation of $\Omega = 40$ dB, $N = 8$ antennas at the STx, the angles of the users set at $\theta_1^H = 30°$, $\theta_2^H = 50°$, $\theta_1^{ID} = -25°$, and $\theta_2^{ID} = -60°$, data rate requirements from $R_{\min} = 1$ bit/s/Hz to $R_{\min} = 8$ bits/s/Hz, with EH requirements from $\psi = -6$ dBm to $\psi = -24$ dBm. The validation set was composed of 560 samples considering $N = 8$ antennas at the STx, data rate requirements from $R_{\min} = 1$ bit/s/Hz to $R_{\min} = 8$ bits/s/Hz, and EH requirements from $\psi = -6$ dBm to $\psi = -27$ dBm. The testing data were used as described in Section IV.B and were varied based on the case to be analyzed. Note that the testing data were not used during the training and hyperparameter selection processes. Moreover, the training and validation dataset were collected by assuming a perfect CSIT.

A. TUNING THE HYPERPARAMETERS OF THE MODELS

First, we describe the autoencoder, which is composed of three hidden layers with 8, 1, and 8 units in each hidden layer, i.e. J=1. We use the tanh function as the activation function along with the Adam optimizer, where mean absolute error is the loss function. As described in Section III.B, the samples

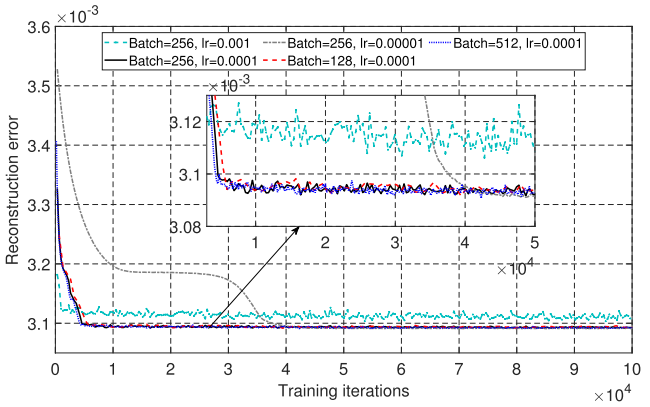

FIGURE 6. Convergence behavior of the autoencoder.

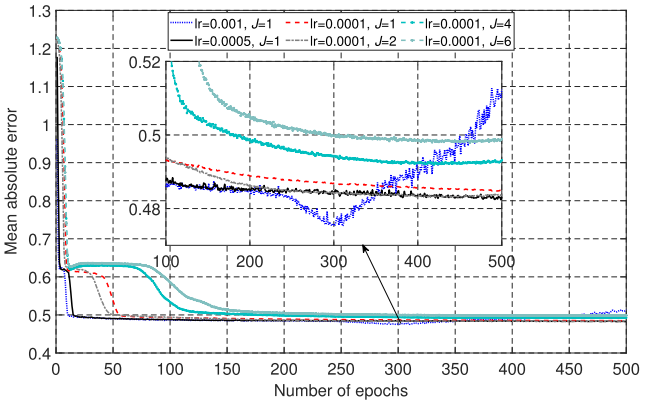

FIGURE 7. Convergence behavior of the DNN based on the learning rate and J.

of the dataset for the autoencoder were the channel vectors, which could be $\mathbf{h}_u$, $\mathbf{q}_d$, or $\mathbf{g}_k$. In particular, we used a training dataset composed of 84,000 channel vectors and a validation set of 12,000 channels. The channel vectors were generated considering $N = 8$ antennas at the STx. Note that this dataset can easily be obtained because the autoencoder is an unsupervised learning method and does not require any labels for training. To simplify the presentation of the results, we considered the parameters of the learning rate (lr), the batch size, and the number of epochs. However, other types of activation function, numbers of hidden layers, and units were analyzed in order to select the best hyperparameters.

Fig. 6 shows the convergence behavior of the autoencoder for several combinations of batch size and learning rate, where training iterations represented the process to update the weights in the autoencoder through the backpropagation algorithm. For instance, with a batch size of 256 and 84000 training samples, 329 training iterations were executed in each epoch. Increasing the batch size means that more samples were used to accurately estimate the error gradient in each step, which allowed the model to converge in fewer iterations. However, as the batch size increases, more machine memory is required. Moreover, we observed that as the learning rate increased, faster convergence was achieved, but not even the slightest reconstruction error was reached. On the other hand, a very low learning rate presented low convergence. Then, we selected a learning rate equal to 0.0001, a batch size of 256, and 200 epochs.

The DNN is composed of three hidden layers with 100 units in each. The activation function was the exponential linear unit (ELU) function along with the Adam optimizer, with mean absolute error as the loss function. Moreover, we shuffled the training data before each epoch. Fig. 7 shows the convergence behavior of the DNN with a batch size of 256 for different values of learning rate and J. We observe that a high learning rate involved fast convergence, but caused overfitting. On the other hand, a very low learning rate had slow convergence and required more epochs to achieve convergence. Moreover, we investigated the effect of the number of units in the middle layer of the autoencoder (J).

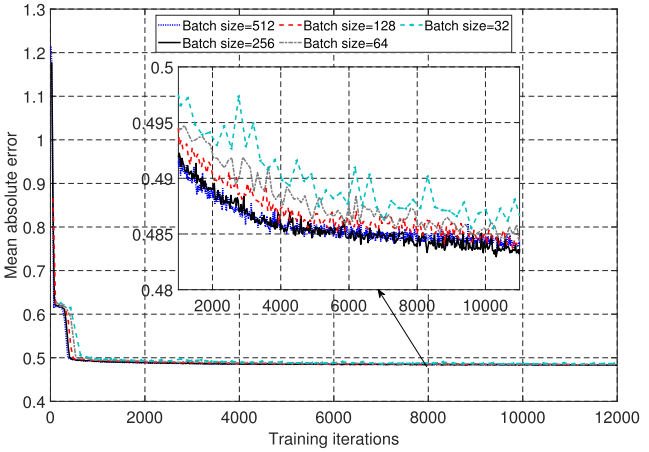

FIGURE 8. Convergence behavior of the DNN based on the batch size.

In the case of an autoencoder with $J = 2$, the best structure for the DNN was three hidden layers with 150 units in each. Concerning the case of the autoencoders with $J = 4$ and $J = 6$, the best structure for the DNN was four hidden layers with 50 units in each. We see that the schemes with $J = 1$ and $J = 2$ achieve similar results with $J = 1$ having fewer trainable parameters. In addition, we observe that as we increase the value of J, less is the generalization ability of the DNN.

Fig. 8 compares convergence of the DNN for different batch sizes with a learning rate of 0.0005. Similar to Fig. 6, as we increase the batch size, faster is the convergence. We observe that the batch sizes of 256 and 512 achieve the lowest error with a batch size of 256 requiring less machine memory. Then, we selected $J = 1$, a learning rate equal to 0.0005, a batch size of 256, and 200 epochs for the rest of the simulations.

B. PERFORMANCE ANALYSIS OF THE PROPOSED APPROACH

In this subsection, the presented results are averaged over several channel realizations. Moreover, we averaged the

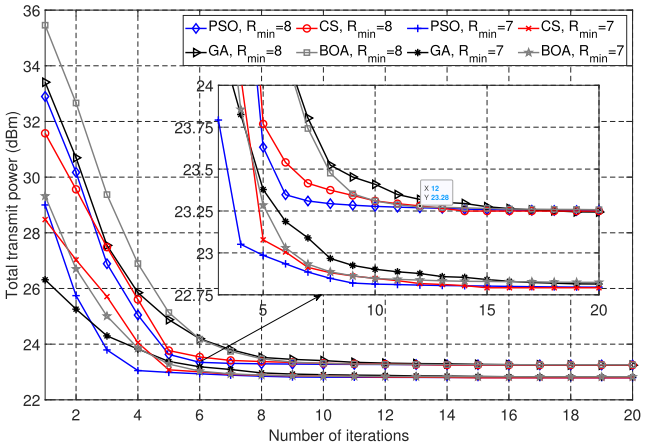

FIGURE 9. Convergence behavior of the comparative schemes.

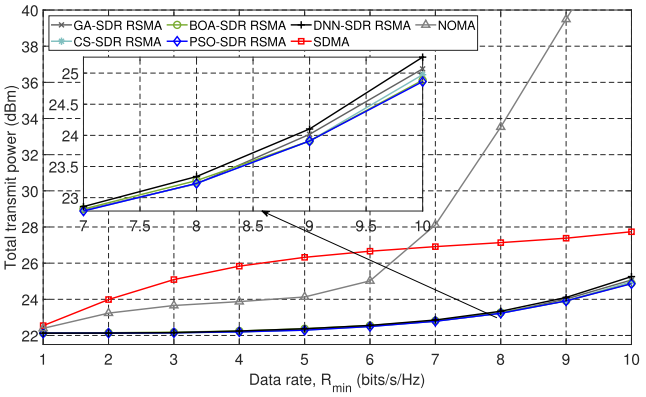

FIGURE 10. Total transmit power at the STx according to the data rate requirement.

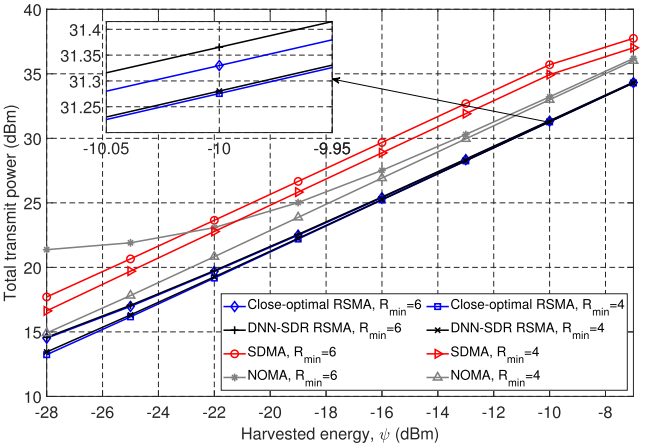

FIGURE 11. Total transmit power at the STx according to the EH requirement.

results obtained with several DNNs, each of them trained with the same dataset but with different initial weights.

In our simulations, the main parameters of the iterative-based schemes are $N_{PSO} = N_{GA} = N_{CS} = N_{BOA} = 10$, and $I_{PSO}^{\max} = I_{GA}^{\max} = I_{CS}^{\max} = I_{BOA}^{\max} = 20$. Fig. 9 shows the convergence behavior of the comparative schemes for RSMA when an EH requirement of $\psi = -19$ dBm is given. We see that all the iterative-based schemes converge within 20 iterations and achieve a similar transmission power. Moreover, the PSO-based scheme converges faster than the other iterative-based schemes, while achieving the lowest transmission power.

In Fig. 10 and Fig. 11, the testing data were composed of samples with a signal attenuation of $\Omega = 40$ dB, $N = 8$ antennas at the STx, and angles of the users at $\theta_1^H = -15°$, $\theta_2^H = -70°$, $\theta_1^{ID} = 80°$, and $\theta_2^{ID} = 10°$. Fig. 10 shows the transmit power at the STx according to the data rate requirement for the hybrid and ID users when a minimum EH of $\psi = -19$ dBm is given. We observe that the proposed DNN–SDR approach achieves a very close performance to those of the comparative iterative methods with less computational complexity. Moreover, the schemes developed with the RSMA technique achieved lower transmission power, compared with the traditional SDMA and NOMA. The increase in the gap between the proposed DNN-SDR approach and the PSO-SDR RSMA method at rate requirements higher than $R_{\min} = 8$ bits/s/Hz is because $R_{\min} = 9$ bits/s/Hz and $R_{\min} = 10$ bits/s/Hz are new scenarios never seen in the training and validation data. The improvement of NOMA over SDMA is because NOMA performs SIC to decode the interference caused by other secondary users' messages, which increases the achievable rate for the secondary users while reducing the required transmission power. However, as the rate requirement increases, more transmission power needs to be allocated to each user's message. In particular, the closer user needs to decode the message of the farther user through SIC, which requires increasing the transmission power for the message of the farther user. Then, for high-rate requirements, the SDMA scheme had better performance, compared to NOMA, since more directive beams can be obtained by optimizing the precoder vectors. In the rest of this Section, we denote the PSO-based scheme with RSMA as Close-optimal RSMA for comparison purposes.

Fig. 11 provides comparisons of the total transmit power at the STx according to the minimum required EH at the hybrid users for minimum data rate requirements of $R_{\min} = 4$ bits/s/Hz and $R_{\min} = 6$ bits/s/Hz. As expected, both RSMA methods outperformed the SDMA and NOMA schemes in terms of minimum transmit power. Note that the proposed scheme based on the DNN achieved results similar to the close-to-optimal RSMA but with a significant reduction in computational complexity. Thus, we proved the superiority of the RSMA method over the conventional SDMA and NOMA schemes in the proposed system model, where RSMA is established in the literature as a general multiple access method, with SDMA and NOMA as particular cases [2], [3]. For instance, the SDMA strategy can be applied by setting the precoder vector of the common stream to zero, which means that message m_u^H is directly encoded into s_u^H, and m_d^{ID} is directly encoded into s_d^{ID}. The slight decrease on

TABLE 2. Comparison of computational time.

Method	Close-to-optimal RSMA	DNN–SDR RSMA	NOMA	SDMA
Time [s]	61.0490	0.8703	0.8195	0.7335

the performance of the DNN-SDR approach at $R_{\min} = 6$ bits/s/Hz compared with the case of $R_{\min} = 4$ bits/s/Hz is because the DNN predicts the value of the common rate variables $\left\{r_{u,c}^{H}, r_{d,c}^{ID}\right\}$ of which upper limits are defined by their corresponding $\left\{R_{u,\min}^{H}, R_{d,\min}^{ID}\right\}$ as detailed in (15a) and (15b). Therefore, as $R_{\min}$ increases, more are the possible values for the common rate variables leading to a slight increase in the prediction error. However, the difference in the performance of the DNN-SDR approach compared with that of the close-optimal RSMA for rate requirements lower than $R_{\min} = 8$ bits/s/Hz is very small as we can observe in Fig. 10.

Table 2 shows the computational time achieved by the comparison methods with eight antennas at the STx. We consider several channel realizations with different values for rate and EH requirements, where we report the average computational time. Moreover, all the considered schemes are subject to the same channel vectors and system parameters to guarantee a fair comparison. As described in Section III.B, the proposed scheme is composed of the training phase and deployment phase, where the computational time of the training phase is not included in Table 2 because it is performed in offline before the deployment phase. Then, the computational time for the proposed DNN-SDR scheme is composed of the computational time of the DNN module given by 0.0975s and the computational time to solve the problem (18) given by 0.7728s. We observe that the proposed DNN–SDR approach can reduce the computational time about 70-fold, compared with the close-to-optimal method, while achieving similar performance. Moreover, the computational complexity of the DNN–SDR scheme is only slightly higher than SDMA and NOMA, while providing a significant improvement. In the results shown in Table 2, the penalty method was not necessary, since all the matrices were rank-one. In general, concerning the results presented in this section, only 1.2% of the cases needed the penalty method where only one iteration was required in most of the cases.

Now, we study the generalization performance of the proposed scheme for scenarios that are different from the ones used in the training data, such as different signal attenuations, different numbers of transmitting antennas at the STx, and imperfect CSIT. Fig. 12 shows the transmit power at the STx versus the signal attenuation for the hybrid and ID users subject to an EH requirement of $\psi = -19$ dBm and a rate requirement of $R_{\min} = 6$ bits/s/Hz. The test data were composed of signal attenuations from $\Omega = 36$ dB to $\Omega = 50$ dB, $N = 8$ antennas at the STx, and angles of users set at $\theta_1^H = -15°$, $\theta_2^H = -70°$, $\theta_1^{ID} = 80°$, and $\theta_2^{ID} = 10°$. We see that the proposed DNN-based scheme had performance similar to the close-to-optimal approach while reaching a significant improvement over the NOMA and SDMA methods. Note that the DNN and autoencoder were trained by using samples with a signal attenuation of $\Omega = 40$ dB, and then, the proposed scheme proved to be robust to diverse signal attenuations.

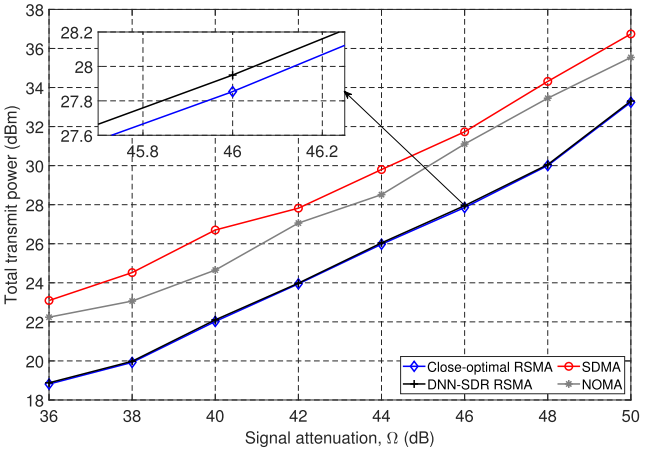

FIGURE 12. Total transmit power at the STx versus signal attenuation.

Fig. 13 illustrates the transmit power at the STx versus the number of transmitting antennas subject to an EH requirement of $\psi = -15$ dBm and a rate requirement of $R_{\min} = 6$ bits/s/Hz. The test data were composed of signal attenuation $\Omega = 40$ dB, numbers of antennas at the STx ranging from $N = 6$ to $N = 28$, and angles of users at $\theta_1^H = -15°$, $\theta_2^H = -70°$, $\theta_1^{ID} = 80°$, and $\theta_2^{ID} = 10°$. This is a challenging scenario, because as the number of antennas increases, more elements are presented in the channel vector modifying the input dimension of the samples. As mentioned in Section III.B, we kept the same DNN module for all the number of antennas, and only trained a new autoencoder for new numbers of antennas while keeping the same dimension in the middle layer. For instance, with $N = 28$ antennas, we used an autoencoder composed of three hidden layers with 28, 1, and 28 units in each hidden layer for the case of DNN-SDR RSMA with $J = 1$ while using the same DNN as the case of $N = 8$ antennas. Moreover, training an autoencoder is a relatively easy task since the same input is used as output. For comparison purposes, we included the schemes with $J = 2$ and $J = 4$, each of them having an indenpendent DNN with a structure detailed in Subsection IV.A. We observed that the proposed scheme can adapt to challenging scenarios while achieving a result similar to the close-to-optimal approach. In addition, we see that at $N = 8$ antennas, the schemes $J = 1$, $J = 2$, and $J = 4$ had similar results. However, at $N = 28$ antennas the schemes of $J = 1$ and $J = 2$ achieve a lower transmit power compared with the scheme of $J = 4$, which is consistent with the results obtained in Fig. 7. It is worth highlighting that the training data only considered samples with $N = 8$ antennas, which proves the generalization capability of the proposed approach for very different scenarios.

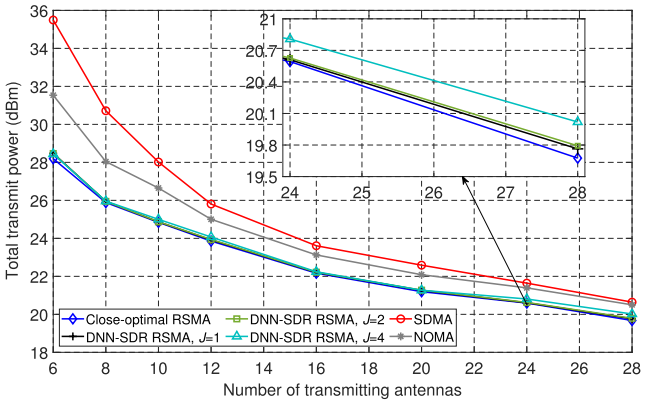

FIGURE 13. Total transmit power at the STx versus the number of transmitting antennas.

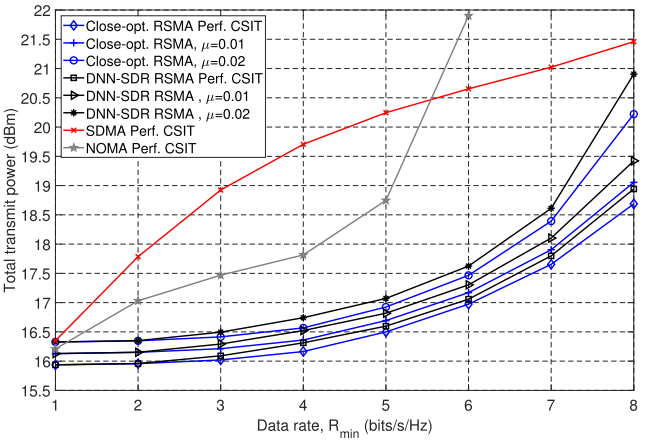

FIGURE 14. Total transmit power at the STx versus the data rate requirement when imperfect CSIT is considered.

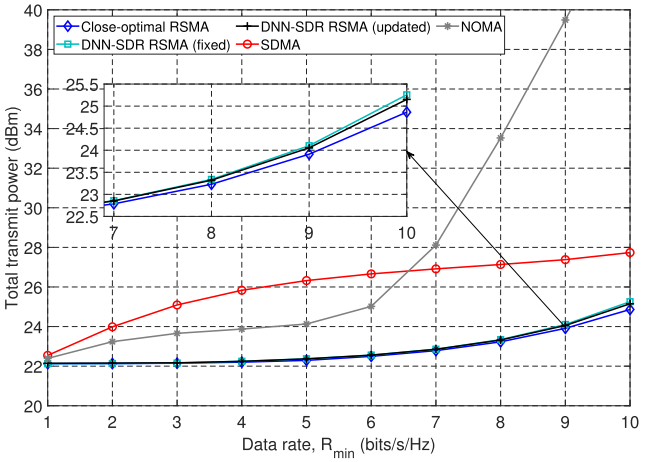

FIGURE 15. Total transmit power vs. data rate requirements after fine tuning.

Finally, we study the generalization performance with imperfect CSIT. The radii of the channel errors are defined as $\varepsilon_{\mathbf{h},u} = \mu_{\mathbf{h},u}\left\|\hat{\mathbf{h}}_u\right\|_2$, $\varepsilon_{\mathbf{q},d} = \mu_{\mathbf{q},d}\left\|\hat{\mathbf{q}}_d\right\|_2$, $\varepsilon_{\mathbf{g},k} = \mu_{\mathbf{g},k}\left\|\hat{\mathbf{g}}_k\right\|_2$, where $\mu_{\mathbf{h},u} = \mu_{\mathbf{q},d} = \mu_{\mathbf{g},k} = \mu$, $\mu \in [0, 1)$ are the relative value of CSI uncertainties. Fig. 14 shows the transmit power at the STx according to the rate requirement subject to different levels of imperfect CSIT with an EH requirement of $\psi = -25$ dBm. This is a very difficult scenario to prove the generalization performance since the training and validation datasets were collected by assuming a perfect CSIT and do not contain samples with imperfect CSIT and EH requirement of $\psi = -25$ dBm. We see that the transmission power increases according to the value of the CSI uncertainties. The reason is that the considered model for imperfect CSIT leads to optimizing a robust beamforming problem to satisfy the worst-case user requirements. Then, as the level of imperfect CSIT increases, higher is the effect of the worst-case user requirements, which increases the required transmission power. We observed that the proposed DNN-based scheme can successfully deal with imperfect CSIT scenarios while achieving a result similar to the close-to-optimal approach. Moreover, we see that RSMA with imperfect CSIT achieves a significantly lower transmission power than SDMA and NOMA with perfect CSIT for the considered rate requirements.

C. THE FINE-TUNING PROCESS

Fine tuning is based on retraining the weights of the final DNN to adapt the model to a new working condition. We applied fine tuning to improve the performance of the proposed scheme in scenarios never seen during the training process. The general procedure is to use the weights of the final DNN as initial weights in order to execute the backpropagation procedure with the new training data collected for the new scenario. This procedure permits us to have a scheme with better performance for the new scenario by collecting relatively few samples, since we used a pre-trained model as the initial point.

Fig. 15 shows the transmit power at the STx according to the data rate requirements, with a minimum EH of $\psi = -19$ dBm, and where the DNN model after the fine-tuning process is denoted as DNN–SDR RSMA (updated). The fine-tuning procedure used a learning rate of 0.0005, and a batch size of 128 with 10 epochs. The new training data consisted of 1900 samples with data rate requirements of $R_{\min} = 9$ bits/s/Hz and $R_{\min} = 10$ bits/s/Hz, and EH requirements from $\psi = -10$ dBm to $\psi = -25$ dBm. The objective of fine tuning is to improve the performance for scenarios with rate requirements of $R_{\min} = 9$ bits/s/Hz and $R_{\min} = 10$ bits/s/Hz. We observed from the fine-tuning procedure that a slight improvement was achieved, compared with the case of fixed weights.

Fig. 16 shows the transmit power at the STx according to the EH requirements with a rate requirement of $R_{\min} = 6$ bits/s/Hz and $N = 24$ antennas. The fine-tuning procedure used a learning rate of 0.0001, a batch size of 256, and 10 epochs. The new training data consisted of 2000 samples with $N = 24$ antennas, data rate requirements from $R_{\min} = 3$ bits/s/Hz to $R_{\min} = 10$ bits/s/Hz, and EH requirements from $\psi = -7$ dBm to $\psi = -25$ dBm. We see that the fine-tuning process permits an improvement over the case with fixed

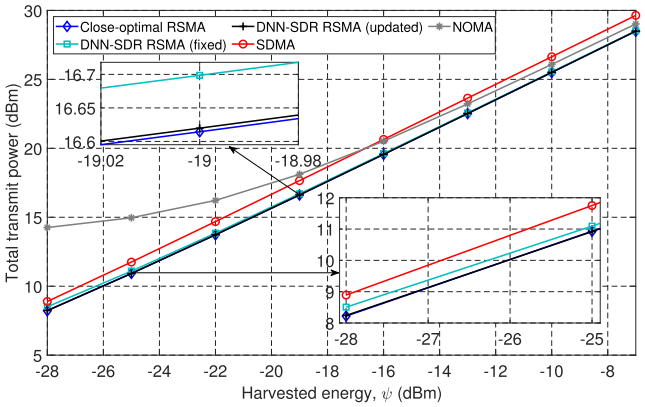

FIGURE 16. Total transmit power vs. EH requirements with $N = 24$ antennas after fine tuning.

weights, since the weights of the DNN were optimized to the new scenario. Then, by using the fine-tuning procedure, we can adapt the trained DNN to new scenarios without the need to collect very much new data.

V. CONCLUSION

In this paper, we considered a multi-user underlying MISO SWIPT system with RSMA by considering hybrid users and ID users. The precoder vectors, common rate variables, and PS ratios were optimized to minimize the total transmission power at the STx, subject to rate, energy, and interference constraints. The minimum transmit power problem was divided into two subproblems, where the outer problem was solved with a DNN-based scheme with an autoencoder, and the inner problem was solved with the SDR technique. To guarantee feasible results, a penalty function was applied along with the SDR technique. Simulation results showed that the proposed DNN–SDR scheme achieved performance superior to the conventional SDMA and NOMA methods, and performance comparable to the close-to-optimal approach, with a significant reduction in the computational complexity. We showed that the proposed scheme, aided with an autoencoder, has excellent generalization performance to deal with new conditions, such as different signal attenuations, different numbers of transmitting antennas, and imperfect CSIT, without the need to modify the main DNN module. Moreover, we presented the fine-tuning process as a useful method to improve the performance of the proposed framework in new scenarios.

REFERENCES

[1] B. Clerckx, H. Joudeh, C. Hao, M. Dai, and B. Rassouli, "Rate splitting for MIMO wireless networks: A promising PHY-layer strategy for LTE evolution," *IEEE Commun. Mag.*, vol. 54, no. 5, pp. 98–105, May 2016.

[2] Y. Mao, B. Clerckx, and V. O. K. Li, "Rate-splitting multiple access for downlink communication systems: Bridging, generalizing, and outperforming SDMA and NOMA," *EURASIP J. Wireless Commun. Netw.*, vol. 2018, no. 1, pp. 1–54, May 2018.

[3] B. Clerckx, Y. Mao, R. Schober, and H. V. Poor, "Rate-splitting unifying SDMA, OMA, NOMA, and multicasting in MISO broadcast channel: A simple two-user rate analysis," *IEEE Wireless Commun. Lett.*, vol. 9, no. 3, pp. 349–353, Mar. 2020.

[4] O. Dizdar, Y. Mao, W. Han, and B. Clerckx, "Rate-splitting multiple access: A new frontier for the PHY layer of 6G," in *Proc. IEEE 92nd Veh. Technol. Conf. (VTC-Fall)*, Nov. 2020, pp. 1–7.

[5] S. Mao, S. Leng, J. Hu, and K. Yang, "Power minimization resource allocation for underlay MISO-NOMA SWIPT systems," *IEEE Access*, vol. 7, pp. 17247–17255, 2019.

[6] H. Sun, F. Zhou, R. Q. Hu, and L. Hanzo, "Robust beamforming design in a NOMA cognitive radio network relying on SWIPT," *IEEE J. Sel. Areas Commun.*, vol. 37, no. 1, pp. 142–155, Jan. 2019.

[7] T. D. P. Perera, D. N. K. Jayakody, S. K. Sharma, S. Chatzinotas, and J. Li, "Simultaneous wireless information and power transfer (SWIPT): Recent advances and future challenges," *IEEE Commun. Surveys Tuts.*, vol. 20, no. 1, pp. 264–302, 1st Quart., 2018.

[8] S. Bi, C. K. Ho, and R. Zhang, "Wireless powered communication: Opportunities and challenges," *IEEE Commun. Mag.*, vol. 53, no. 4, pp. 117–125, Apr. 2015.

[9] Q. Shi, L. Liu, W. Xu, and R. Zhang, "Joint transmit beamforming and receive power splitting for MISO SWIPT systems," *IEEE Trans. Wireless Commun.*, vol. 13, no. 6, pp. 3269–3280, Jun. 2014.

[10] A. Dong, H. Zhang, D. Wu, and D. Yuan, "QoS-constrained transceiver design and power splitting for downlink multiuser MIMO SWIPT systems," in *Proc. IEEE Int. Conf. Commun. (ICC)*, May 2016, pp. 1–6.

[11] J. Tang, D. K. C. So, N. Zhao, A. Shojaeifard, and K.-K. Wong, "Energy efficiency optimization with SWIPT in MIMO broadcast channels for Internet of Things," *IEEE Internet Things J.*, vol. 5, no. 4, pp. 2605–2619, Aug. 2018.

[12] H. M. Al-Obiedollah, K. Cumanan, J. Thiyagalingam, A. G. Burr, Z. Ding, and O. A. Dobre, "Energy efficient beamforming design for MISO non-orthogonal multiple access systems," *IEEE Trans. Commun.*, vol. 67, no. 6, pp. 4117–4131, Jun. 2019.

[13] Y. Xu, C. Shen, Z. Ding, X. Sun, S. Yan, and G. Zhu, "Joint beamforming design and power splitting control in cooperative SWIPT NOMA systems," in *Proc. IEEE Int. Conf. Commun. (ICC)*, May 2017, pp. 1–6.

[14] Q. Li and L. Yang, "Robust optimization for energy efficiency in MIMO two-way relay networks with SWIPT," *IEEE Syst. J.*, vol. 14, no. 1, pp. 196–207, Mar. 2020.

[15] J. Liao, M. R. A. Khandaker, and K.-K. Wong, "Robust power-splitting SWIPT beamforming for broadcast channels," *IEEE Commun. Lett.*, vol. 20, no. 1, pp. 181–184, Jan. 2016.

[16] S. Boyd, L. E. Ghaoui, E. Ferron, and V. Balakrishnan, *Linear Matrix Inequalities in System and Control Theory*. Philadelphia, PA, USA: SIAM, 1994.

[17] L. Mohjazi, I. Ahmed, S. Muhaidat, M. Dianati, and M. Al-Qutayri, "Downlink beamforming for SWIPT multi-user MISO underlay cognitive radio networks," *IEEE Commun. Lett.*, vol. 21, no. 2, pp. 434–437, Feb. 2017.

[18] P. V. Tuan and I. Koo, "Optimal multiuser MISO beamforming for power-splitting SWIPT cognitive radio networks," *IEEE Access*, vol. 5, pp. 14141–14153, 2017.

[19] C. E. Garcia, M. R. Camana, and I. Koo, "Joint beamforming and artificial noise optimization for secure transmissions in MISO-NOMA cognitive radio system with SWIPT," *Electronics*, vol. 9, no. 11, p. 1948, Nov. 2020.

[20] F. Zhou, Z. Chu, H. Sun, R. Q. Hu, and L. Hanzo, "Artificial noise aided secure cognitive beamforming for cooperative MISO-NOMA using SWIPT," *IEEE Trans. J. Sel. Areas. Commum.*, vol. 36, no. 4, pp. 918–931, Apr. 2018.

[21] C. E. Garcia, M. R. Camana, and I. Koo, "Relay selection and power allocation for secrecy sum rate maximization in underlying cognitive radio with cooperative relaying NOMA," *Neurocomputing*, vol. 452, pp. 756–767, Sep. 2021.

[22] H. Joudeh and B. Clerckx, "Robust transmission in downlink multiuser MISO systems: A rate-splitting approach," *IEEE Trans. Signal Process.*, vol. 64, no. 23, pp. 6227–6242, Dec. 2016.

[23] M. Dai, B. Clerckx, D. Gesbert, and G. Caire, "A rate splitting strategy for massive MIMO with imperfect CSIT," *IEEE Trans. Wireless Commun.*, vol. 15, no. 7, pp. 4611–4624, Jul. 2016.

[24] Y. Mao, B. Clerckx, and V. O. K. Li, "Rate-splitting for multi-antenna non-orthogonal unicast and multicast transmission: Spectral and energy efficiency analysis," *IEEE Trans. Commun.*, vol. 67, no. 12, pp. 8754–8770, Dec. 2019.

[25] Y. Mao, B. Clerckx, and V. O. K. Li, "Energy efficiency of rate-splitting multiple access, and performance benefits over SDMA and NOMA," in *Proc. 15th Int. Symp. Wireless Commun. Syst. (ISWCS)*, Aug. 2018, pp. 1–6.

[26] G. Zhou, Y. Mao, and B. Clerckx, "Rate-splitting multiple access for multi-antenna downlink communication systems: Spectral and energy efficiency tradeoff," *IEEE Trans. Wireless Commun.*, early access, Dec. 14, 2021, doi: 10.1109/TWC.2021.3133433.
[27] Y. Mao, B. Clerckx, and V. O. K. Li, "Rate-splitting for multi-user multi-antenna wireless information and power transfer," in *Proc. IEEE 20th Int. Workshop Signal Process. Adv. Wireless Commun. (SPAWC)*, Jul. 2019, pp. 1–5.
[28] X. Su, L. Li, H. Yin, and P. Zhang, "Robust power- and rate-splitting-based transceiver design in K-user MISO SWIPT interference channel under imperfect CSIT," *IEEE Commun. Lett.*, vol. 23, no. 3, pp. 514–517, Mar. 2019.
[29] M. R. Camana, P. V. Tuan, C. E. Garcia, and I. Koo, "Joint power allocation and power splitting for MISO SWIPT RSMA systems with energy-constrained users," *Wireless Netw.*, vol. 26, no. 3, pp. 2241–2254, Aug. 2019.
[30] M. R. C. Acosta, C. E. G. Moreta, and I. Koo, "Joint power allocation and power splitting for MISO-RSMA cognitive radio systems with SWIPT and information decoder users," *IEEE Syst. J.*, vol. 15, no. 4, pp. 5289–5300, Dec. 2021.
[31] W. Zhang, Z. Zhang, H.-C. Chao, and M. Guizani, "Toward intelligent network optimization in wireless networking: An auto-learning framework," *IEEE Wireless Commun.*, vol. 26, no. 3, pp. 76–82, Jun. 2019.
[32] L. Liang, H. Ye, G. Yu, and G. Y. Li, "Deep-learning-based wireless resource allocation with application to vehicular networks," *Proc. IEEE*, vol. 108, no. 2, pp. 341–356, Feb. 2020.
[33] Q. Wu, T. Ruan, F. Zhou, Y. Huang, F. Xu, S. Zhao, Y. Liu, and X. Huang, "A unified cognitive learning framework for adapting to dynamic environments and tasks," *IEEE Wireless Commun.*, vol. 28, no. 6, pp. 208–216, Dec. 2021.
[34] H. Sun, X. Chen, Q. Shi, M. Hong, X. Fu, and N. D. Sidiropoulos, "Learning to optimize: Training deep neural networks for interference management," *IEEE Trans. Signal Process.*, vol. 66, no. 20, pp. 5438–5453, Oct. 2018.
[35] F. Zhou, X. Zhang, R. Q. Hu, A. Papathanassiou, and W. Meng, "Resource allocation based on deep neural networks for cognitive radio networks," in *Proc. IEEE/CIC Int. Conf. Commun. China (ICCC)*, Aug. 2018, pp. 40–45.
[36] W. Xia, G. Zheng, Y. Zhu, J. Zhang, J. Wang, and A. P. Petropulu, "A deep learning framework for optimization of MISO downlink beamforming," *IEEE Trans. Commun.*, vol. 68, no. 3, pp. 1866–1880, Mar. 2020.
[37] C. C. Aggarwal, *Neural Networks and Deep Learning: A Textbook*, 1st ed. Cham, Switzerland: Springer, 2018.
[38] Z.-Q. Luo, W.-K. Ma, A. M.-C. So, Y. Ye, and S. Zhang, "Semidefinite relaxation of quadratic optimization problems," *IEEE Signal Process. Mag.*, vol. 27, no. 3, pp. 20–34, Apr. 2010.
[39] M. C. Grant and S. P. Boyd. (Mar. 2021). *CVX: MATLAB Software for Disciplined Convex Programming*. [Online]. Available: http://cvxr.com/cvx/
[40] S. Boyd and L. Vandenberghe, *Convex Optimization*. Cambridge, U.K.: Cambridge Univ. Press, 2004.
[41] A. H. Phan, H. D. Tuan, H. H. Kha, and D. T. Ngo, "Nonsmooth optimization for efficient beamforming in cognitive radio multicast transmission," *IEEE Trans. Signal Process.*, vol. 60, no. 6, pp. 2941–2951, Jun. 2012.
[42] P. V. Tuan, P. N. Son, T. T. Duy, S. Q. Nguyen, V. Q. B. Ngo, D. V. Quang, and I. Koo, "Optimizing a secure two-way network with non-linear SWIPT, channel uncertainty, and a hidden eavesdropper," *Electronics*, vol. 9, no. 8, p. 1222, Jul. 2020.
[43] K.-Y. Wang, A. M.-C. So, T.-H. Chang, W.-K. Ma, and C.-Y. Chi, "Outage constrained robust transmit optimization for multiuser MISO downlinks: Tractable approximations by conic optimization," *IEEE Trans. Signal Process.*, vol. 62, no. 21, pp. 5690–5705, Nov. 2014.
[44] R. L. Haupt and S. E. Haupt, *Practical Genetic Algorithms*. 2nd ed. Hoboken, NJ, USA: Wiley, 2004, pp. 27–66.
[45] C. E. Garcia, M. R. Camana, and I. Koo, "Low-complexity PSO-based resource allocation scheme for cooperative non-linear SWIPT-enabled NOMA," *IEEE Access*, vol. 10, pp. 34207–34220, 2022.
[46] M. O. Okwu and L. K. Tartibu, *Metaheuristic Optimization: Nature-Inspired Algorithms Swarm and Computational Intelligence, Theory and Applications*, vol. 927. Cham, Switzerland: Springer, 2020.
[47] E. Karipidis, N. D. Sidiropoulos, and Z. Q. Luo, "Far-field multicast beamforming for uniform linear antenna arrays," *IEEE Trans. Signal Process.*, vol. 55, no. 10, pp. 4916–4927, Oct. 2007.

MARIO R. CAMANA (Graduate Student Member, IEEE) received the B.E. degree in electronics and telecommunications engineering from the Escuela Politécnica Nacional (EPN), Quito, in 2016. He is currently a Graduate Research Assistant with the Department of Electrical, Electronic and Computer Engineering, University of Ulsan, Ulsan, South Korea. His research interests include machine learning, optimizations, and MIMO communications.

CARLA E. GARCIA (Graduate Student Member, IEEE) received the B.E. degree in electronics and telecommunications engineering from the Escuela Politécnica Nacional (EPN), Ecuador, in 2016, and the M.S. degree in electrical engineering from the University of Ulsan, Ulsan, South Korea, in 2020, where she is currently pursuing the Ph.D. degree with the Department of Electrical, Electronic and Computer Engineering. Her main research interests include artificial intelligence, security, MIMO communications, and optimizations.

INSOO KOO received the B.E. degree from Kon-Kuk University, Seoul, South Korea, in 1996, and the M.Sc. and Ph.D. degrees from the Gwangju Institute of Science and Technology (GIST), Gwangju, Korea, in 1998 and 2002, respectively.

From 2002 to 2004, he was a Research Professor at the Ultrafast Fiber-Optic Networks Research Center, GIST. In 2003, he was a Visiting Scholar at the Royal Institute of Science and Technology, Stockholm, Sweden. In 2005, he joined the University of Ulsan, Ulsan, South Korea, where he is currently a Full Professor. His current research interests include spectrum sensing issues for CRNs, channel and power allocation for cognitive radios (CRs) and military networks, SWIPT MIMO issues for CRs, MAC and routing protocol design for UW-ASNs, and relay selection issues in CCRNs.